

# HI Galaxy Signatures in the SARAQ MeerKAT Galactic Plane Survey – I. Probing the richness of the Great Attractor Wall across the inner Zone of Avoidance

Nadia Steyn<sup>1,2,\*</sup>, Renée C. Kraan-Korteweg<sup>1</sup>, Sambatriniaina H. A. Rajohnson<sup>1</sup>, Sushma Kurapati<sup>1</sup>, Hao Chen<sup>1,3</sup>, Bradley Frank<sup>4,5,6,1</sup>, Paolo Serra<sup>7</sup>, Lister Staveley-Smith<sup>2,8</sup>, Fernando Camilo<sup>5</sup>, and Sharmila Goedhart<sup>5,9</sup>

<sup>1</sup> Department of Astronomy, University of Cape Town, Private Bag X3, Rondebosch 7701, South Africa

<sup>2</sup> International Centre for Radio Astronomy Research (ICRAR), The University of Western Australia, 35 Stirling Highway

<sup>3</sup> Research Center for Intelligent Computing Platforms, Zhejiang Laboratory, Hangzhou 311100, China

<sup>4</sup> UK Astronomy Technology Centre, Royal Observatory Edinburgh, Blackford Hill, Edinburgh EH9 3HJ, UK

<sup>5</sup> South African Radio Astronomy Observatory (SARAQ), 2 Fir Street, Observatory, 7925, South Africa

<sup>6</sup> The Inter-University Institute for Data Intensive Astronomy (IDIA), and University of Cape Town, Private Bag X3, Rondebosch, 7701, South Africa

<sup>7</sup> INAF – Osservatorio Astronomico di Cagliari, Via della Scienza 5, 09047, Selargius, CA, Italy

<sup>8</sup> ARC Centre of Excellence for All Sky Astrophysics in 3 Dimensions (ASTRO 3D), Australia

<sup>9</sup> SKAO, 2 Fir Street, Black River Park, Second Floor, Block A, Cape Town, 7925

Accepted XXX. Received YYY; in original form ZZZ

## ABSTRACT

This paper presents the first HI results extracted from the SARAQ MeerKAT Galactic Plane Survey (SMGPS) – a narrow strip ( $\Delta b \sim 3^\circ$ ) along the southern Milky Way. The primary goal consisted in tracing the Great Attractor (GA) Wall across the innermost Zone of Avoidance. We reduced a segment spanning the longitude range  $302^\circ \leq \ell \leq 332^\circ$  for the redshift range  $z \leq 0.08$ . The superb SMGPS sensitivity ( $\text{rms} = 0.3 - 0.5 \text{ mJy beam}^{-1}$  per  $44 \text{ km s}^{-1}$  channel) and angular resolution ( $\sim 31'' \times 26''$ ) lead to a detection limit of  $\log(M_{\text{HI}}/\text{M}_\odot) \geq 8.5$  at the GA distance ( $V_{\text{hel}} \sim 3500 - 6500 \text{ km s}^{-1}$ ). A total of 477 galaxy candidates were identified over the full redshift range. A comparison of the few HI detections with counterparts in the literature (mostly HIZOA) found the HI fluxes and other HI parameters to be highly consistent. The continuation of the GA Wall is confirmed through a prominent overdensity of  $N = 214$  detections in the GA distance range. At higher latitudes, the wall moves to higher redshifts, supportive of a possible link with the Ophiuchus cluster located behind the Galactic Bulge. This deep interferometric HI survey demonstrates the power of the SMGPS in improving our insight of large-scale structures at these extremely low latitudes, despite the high obscuration and continuum background.

**Key words:** surveys – large-scale structure of Universe – galaxies: distances and redshifts – radio lines: galaxies

## 1 INTRODUCTION

The so-called Zone of Avoidance (ZoA) bisects a number of large-scale structures that are relevant for derivations of the motion of the Local Group and bulk flows, e.g., the Local Void (LV; e.g., Kraan-Korteweg et al. 2008; Tully et al. 2019), the Vela Supercluster (SCL; Kraan-Korteweg et al. 2017), and the Great Attractor (GA). The GA was originally discovered from one of the earliest whole-sky peculiar velocity data-sets (Dressler et al. 1987; Lynden-Bell et al. 1988). Matching the GA to an overdensity in galaxies remained a challenge, however, because of its location behind the Milky Way. Dedicated galaxy searches and redshift follow-ups close to the ZoA (Woudt & Kraan-Korteweg 2001; Woudt

et al. 2004; Radburn-Smith et al. 2006) suggested the GA to consist of a large wall-like structure with the rich Norma cluster at its core (ACO 3627;  $\ell, b, V_{\text{hel}} = 325^\circ 3, -7^\circ 2, 4871 \text{ km s}^{-1}$ ; Kraan-Korteweg et al. 1996; Woudt et al. 2004). But these could not penetrate the latitudes below  $|b| \lesssim 5^\circ$ , and the prominence and shape of the Wall across the inner ZoA was never fully ascertained. Only systematic HI surveys prevail at these latitudes, since they are unaffected by obscuration – as first demonstrated by Henning (1992). This was one of the reasons the Parkes HI ZoA survey was conceived ( $212^\circ \leq \ell \leq 36^\circ, b \leq \pm 5^\circ; V_{\text{hel}} < 12700 \text{ km s}^{-1}$ ; Staveley-Smith et al. 2016, henceforth HIZOA). With a  $15.5''$  beam size and  $6 \text{ mJy beam}^{-1} \text{ chan}^{-1}$  noise (rms), it was optimised to uncover normal spirals at the GA distance range. And indeed HIZOA succeeded in tracing the GA across the optically opaque part of the ZoA, albeit with the low detection rate of  $\sim 1$  galaxy per  $2 \text{ deg}^2$  on average. How-

\* E-mail: nadia.steyn@icrar.org

ever, the single dish data became increasingly incomplete where the continuum background rises above  $T_B > 7\text{K}$  ( $|b| \lesssim 1^\circ 5$ ), reaching zero completeness for  $T_B > 16\text{K}$ .

The SARAO MeerKAT Galactic Plane Survey (SMGPS; Goedhart et al., in prep) is ideally suited to bridge this gap. The interferometric data will be less affected by continuum residuals due to spatial filtering. Moreover, the typically  $\sim 1$  hr on-source integration per pointing leads to a sensitivity of  $0.3\text{--}0.5\text{ mJy beam}^{-1}$  per  $44\text{ km s}^{-1}$  channel – an order of magnitude better than HIZOA – while the spatial resolution of  $\sim 31'' \times 26''$  ( $15.5'$  in HIZOA) will resolve all galaxies with HI-masses above  $10^8 M_\odot$  at a typical distance of 70 Mpc, according to the HI mass-size relation of Wang et al. (2016).

This first of a series of papers analysing the SMGPS HI data will zoom in on the GA-Wall ZoA-crossing. Here we cover the longitude range  $302^\circ \leq \ell \leq 332^\circ$ , where the higher longitude side was selected to find signatures for the GA Wall extension emanating from the Norma cluster (e.g., Woudt et al. 2008), while the other end will encompass the surroundings of the galaxy cluster centered on PKS 1343–601 (Nagayama et al. 2004; Schröder et al. 2007).

## 2 OBSERVATIONS

### 2.1 Data Reduction and Imaging

The SMGPS observations were carried out between July 2018 and March 2020 with the MeerKAT L-band receiver and the SKARAB-4k correlator (Goedhart et al., in prep). The 4096 channels across the frequency range 856 – 1712 MHz led to a frequency resolution of 209 kHz, producing a velocity resolution of  $44.1\text{ km s}^{-1}$  at  $z = 0$ .

For this study, we reduced a subsection of the full 528 deg $^2$  SMGPS: a  $30^\circ \times 3^\circ$  survey area comprising 157 pointings arranged in a closely-spaced grid (henceforth the GA-SMGPS pointings). The calibration, imaging and mosaicking were completed on the Ilifu cloud computing facility, hosted by the Inter-University Institute for Data Intensive Astronomy (IDIA). We processed the mostly RFI-free frequency range 1308 – 1430 MHz, using both orthogonal polarizations, but excluded frequencies dominated by gas emission from the Milky Way (1419.46 – 1421.35 MHz). This allows us to investigate the large-scale structure out to  $V_{\text{hel}} < 25000\text{ km s}^{-1}$ ; far enough to include the volume relevant to (residual) bulk flow studies ( $V_{\text{hel}} > 16000\text{ km s}^{-1}$ ; Springob et al. 2016; Scrimgeour et al. 2016), and achieving excellent sensitivity well into the dwarf regime at the distance of the GA overdensity ( $\sim 3500\text{--}6500\text{ km s}^{-1}$ ).

Our visibility data were reduced with CARACal, an automated end-to-end pipeline for radio interferometry data (Józsa et al. 2020) which invokes STIMELA – a Python package based on container technology (Makhathini 2018). The reduction process includes flagging, cross-calibration, self-calibration, Doppler-tracking correction, and continuum subtraction (see Rajohnson et al., in prep, for details).

The latter is particularly important when working in the innermost ZoA, where continuum sources are abundant. This is seen in the top panel of Fig. 1, which displays the 1.4 GHz background continuum temperature, as derived from CHIPASS by Calabretta et al. (2014), extracted here for the GA-SMGPS region. Overlaid in cyan are the positions of the 157 GA-SMGPS pointings with their FWHM radius of  $0^\circ 5$  ( $z=0$ ). The bottom panel shows the colour-coded rms per individual field as determined from the central plane of the respective HI-data cube ( $\langle \text{rms} \rangle = 0.51\text{ mJy}$ ). The slight overall rise in the amplitude of the rms towards higher longitudes is due to an increase in the continuum emission of our Galaxy, while the patches of higher rms show a clear trend with bright emission sources. These are

primarily caused by extended diffuse continuum sources. They raise the receiver temperature locally and may reduce the HI detectability.

The HI data were imaged with WSLEAN, using a pixel scale of  $3''$  and a Briggs robust weighting of  $r = 0$ . We employed a UV-tapering of  $15''$  because the profiles of the non-tapered point spread functions (PSFs, or ‘dirty beams’) revealed significant wings, causing clear deviations from Gaussianity, which would make it difficult to calculate integrated flux. The taper increased the beam size from a mean of  $\sim 11'' \times 9''$  to about  $\sim 31'' \times 26''$ , which is sufficient for our science goals.

### 2.2 Mosaicking

The final HI fields were imaged with  $0.8^\circ$  radii (corresponding to a cut-off at 20% sensitivity) and were primary-beam corrected using the method described in Mauch et al. (2020). These were combined within CARACal into ten consecutive, overlapping HI mosaics, consisting of 22 pointings per mosaic. They are designated as T10 to T19; where “T” is for “tile”, in accordance with SMGPS observation nomenclature. Each mosaic has an on-sky footprint of roughly  $5^\circ \times 3.5^\circ$  (see Fig. 2) with a generous overlap of  $\Delta\ell \sim 2.5^\circ$ . The continuum data were likewise imaged with a pixel size of  $3''$  and constructed into two-dimensional mosaics. The central  $\Delta\ell \sim 3.5^\circ$  of each HI mosaic was used for analysis – a region with near-uniform sensitivity (apart from artefacts) given the hexagonal sampling pattern and small offsets between pointings.

Figure 2 shows the continuum mosaic (left) next to a central HI plane from mosaic T12. Inspecting the HI images for continuum residuals, we found that compact continuum sources overall are well subtracted, but large-scale diffuse continuum sources caused an increase in the noise of the output image (e.g., around  $\ell \gtrsim 325^\circ$ ).

The measured rms of the ten mosaics range from  $0.39\text{--}0.53\text{ mJy}$  (mean mosaic rms =  $0.47\text{ mJy}$ ). This includes the overall increase in  $T_B$  towards higher longitudes and local variations induced by continuum residuals – the latter of which could hamper source extraction. Apart from some remaining Global Positioning Satellites RFI spikes (1376 – 1386 MHz), the spectral baselines within the HI mosaics mostly remain flat out to the edge of the survey ( $V_{\text{hel}} < 25000\text{ km s}^{-1}$ ), with little variation in the noise level.

## 3 SOURCE FINDING

Given the size of mosaics ( $\sim 6600 \times 4300 \times 570$  pixels per  $\sim 65\text{ GB}$  cube), visual source finding becomes prohibitive, and automated source-detection algorithms, such as SoFiA used in this work (Serra et al. 2015; Westmeier et al. 2021), become essential. On the other hand, having an existing source list to optimise the parameter settings is incredibly advantageous. We therefore searched one full mosaic visually using CARTA (Comrie et al. 2021) – a remote image visualisation and analysis tool. We chose T12 as the representative mosaic for the visual search. It lies close to the Wall that seems to be emanating from the Norma Cluster ( $\ell \sim 325^\circ$ ), moreover, its relatively high number of HIZOA detections (12) increases the likelihood of uncovering a fair number of SMGPS HI detections for the optimisation process – and indeed 90 sources were found in T12 alone. The resulting visual catalog was used as a template to optimise the SoFiA v2.3.1 parameter settings.

We chose a central rectangular search area ( $3.5^\circ \times 3.0^\circ$ ) within which to execute SoFiA (see white rectangle in Fig. 2). This was selected to be slightly larger than the longitudinal offset between the mosaics ( $\Delta\ell = 3^\circ$ ) to not miss galaxies at the edges, and to allow for

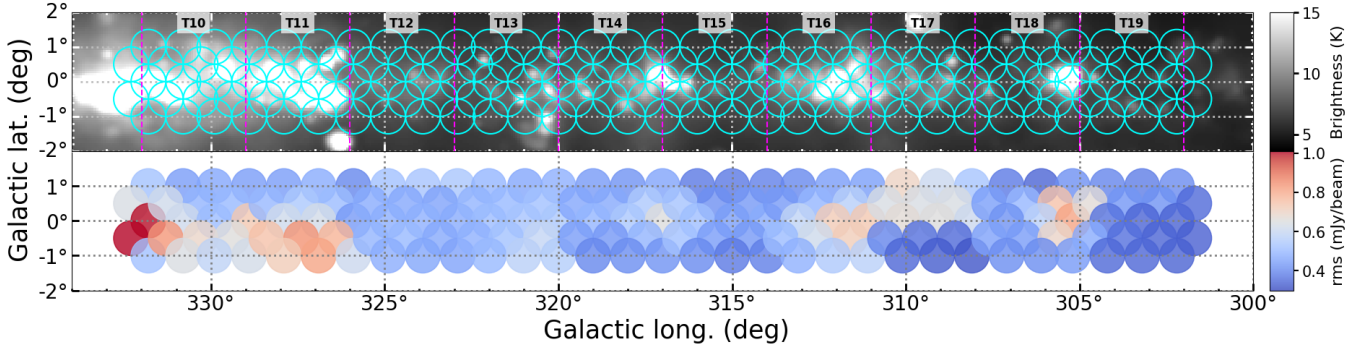


**Figure 1.** Top: The 1.4 GHz radio continuum image based on CHIPASS (Calabretta et al. 2014). The positions of the GA-SMGPS pointings are overlaid in cyan with radii of 0.5 (FWHM at  $z=0$ ). The boundaries separating the mosaics are approximately traced in magenta, with corresponding labels for our mosaic names (explained in text). Bottom: the sensitivity of the GA-SMGPS fields, with colours representing the measured rms of a central plane in the respective field.

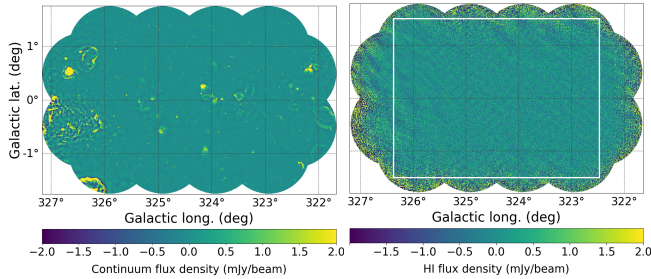


**Figure 2.** Continuum and HI channel map of mosaic T12. The colour scale (linear stretch) indicates the flux variations. While the continuum mosaic reveals both compact and diffuse continuum sources, the centrally located HI plane is – apart from the borders – fairly uniform (rms = 0.42 mJy).

an internal consistency check of source identification and parameter extraction. We cross-matched the visual catalog of T12 to the various outputs from different SoFiA runs, where it became apparent that we required more than one set of parameters to capture the maximum amount of visual detections. This led to an optimised SoFiA source-finding strategy consisting of three consecutive SoFiA runs: in the first run the maximum z-length (`LINKER.MAXSIZEZ`) was set to 21, and was increased in a second run to 31, while the flux threshold (`SCFIND.THRESHOLD`) was changed from  $4.0\sigma$  to  $3.5\sigma$  in the third run. The outputs were merged and false positives removed – being especially critical of detections extracted from noisy regions. Our final parameter settings are available in Appendix A, and further details of the optimisation process can be found in Steyn (2023).

The above-described strategy was implemented on all ten mosaics. The resulting detection lists were adjudicated by more than one member of the team, and combined into one final catalog with the duplicates removed. The adjudication was based on an assessment of the moment maps (total intensity and velocity), the global HI spectrum and its S/N ratio, and also the HI extent in kpc with respect to its redshift and observed HI-rotation. All sources are resolved by minimally two beams.

## 4 RESULTS

### 4.1 The GA-SMGPS Catalog

Here we discuss the final HI-catalog and the quality of the extracted HI parameters. We catalogued a total of 477 galaxy candidates in the GA-SMGPS region: 405 solid detections (marked in the catalog as flag 1)

and 72 with slightly lower confidence (flag 2). Flag two detections are still reasonably strong detections but in higher noise areas or with low S/N, and all candidates are used in analysis. The GA-SMGPS galaxy catalog, given in Appendix B, lists the ID as SMGPS-HI Jhhmmss-ddmmss, the mosaic name, the Galactic coordinates  $\ell$ ,  $b$ , the HI parameters  $S_{\text{peak}}$ ,  $S_{\text{int}}$ ,  $\text{err}_{S_{\text{int}}}$ , rms,  $V_{\text{hel}}$ ,  $W_{20}$ ,  $W_{50}$ ,  $\log M_{\text{HI}}$ , and lastly, flag and note/counterpart. Details are explained in Appendix B. An atlas of all detections (moment maps and HI-profiles) is also available online.

Flux verification and reproducibility is a fundamental step in assessing the data quality of HI images. At these low latitudes, no optical counterparts are known and the primary source that allows for a comparison is HIZOA. A few infrared counterparts identified in literature (three mentioned in HIZOA and six new) are given in the last column of our galaxy catalog (Appendix B). For comparison, the survey parameters of GA-SMGPS, HIZOA and the forthcoming WALLABY survey (Koribalski et al. 2020) are summarised in Table 1.

Forty (out of 42) HIZOA galaxies in the GA-SMGPS data were recovered by SoFiA. The HIZOA galaxy J1532-56 at  $V \sim 1400 \text{ km s}^{-1}$ , identified as a face-on, very extended, ring-like disk in the GA-SMGPS, has no entry in our catalog: the flux per voxel was too low to allow for a robust parameterisation. Earlier observations of this source with the Australian Telescope Compact Array (ATCA; Staveley-Smith et al. 1998) reported on its exceptionally low column density and large HI-disk. Interestingly, the SMGPS data finds the HI-disk to be even more extended than the ATCA FoV. We performed deeper observations with the MeerKAT 32k correlator for further investigations of the properties of this particular source, and results will be presented in a later study. HIZOA source J1534-56A could not be parametrised for the same reason (low column density).

Of the 40 HIZOA sources we recovered, four were resolved into compact galaxy pairs/groups; not surprising given the large beam of the HIZOA survey. The remaining 36 integrated HI-flux values ( $S_{\text{int}}$ ) are plotted in Fig. 3 versus their SMGPS counterparts (black markers). The two additional points (green markers) are based on 12 hr synthesis HI observations with ATCA of galaxies identified in GLIMPSE (Galactic Legacy Infrared Mid-Plane Survey Extraordinaire; Jarrett et al. 2007).

The SMGPS flux errors were calculated using a method similar to Ramatsoku et al. (2016): by determining the variation of fluxes measured in four emission-free areas surrounding the source, over the same extent as the source. Two outliers (HIZOA J1542-55 and J1605-51; open circles) are not used because their HIZOA baselines show

**Table 1.** Survey parameters of GA-SMGPS, HIZOA and WALLABY.

Parameter	GA-SMGPS	HIZOA	WALLABY <sup>†</sup>
Telescope	MeerKAT	Parkes	ASKAP
Date of observations	2018 – 2019	1997 – 2000	2022 – ongoing
Sky coverage	$302^\circ \leq \ell \leq 332^\circ;  b  \leq 1.5^\circ$	$212^\circ \leq \ell \leq 36^\circ;  b  \leq 5^\circ$	$-90^\circ \leq \delta \leq +30^\circ$
Velocity range ( $cz$ )	< 25000 km s $^{-1}$	< 12740 km s $^{-1}$	< 77000 km s $^{-1}$
Velocity resolution	44.1 km s $^{-1}$	27 km s $^{-1}$ *	4 km s $^{-1}$
Angular resolution	$\sim (31'' \times 26'')$	$15.5'$	$\sim 30''$
Integration time pointing $^{-1}$	$\sim 3600$ s	2100 s	$2 \times 8$ hr
Measured rms (per channel)	0.3–0.5 mJy beam $^{-1}$	6 mJy beam $^{-1}$	1.6 mJy beam $^{-1}$
*after Hanning smoothing			
<sup>†</sup> Widefield ASKAP L-band Legacy All-sky Blind surveyY			

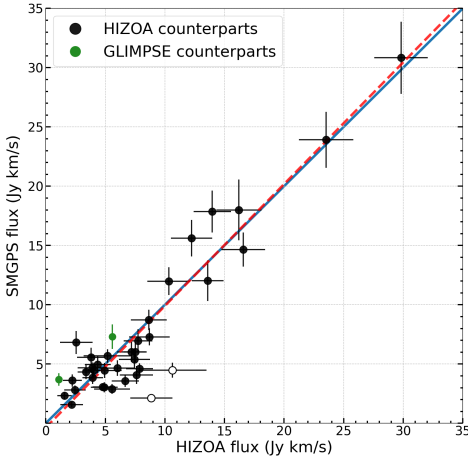


**Figure 3.** Comparison between the integrated fluxes ( $S_{\text{int}}$ ) of GA-SMGPS detections with known counterparts: 36 HIZOA sources and 2 ATCA detections for GLIMPSE galaxies (green). The blue solid line represents a one-to-one relation, the red dashed line a linear fit. Two outliers were excluded from the fit because their HIZOA baselines are unreliable (open circles).

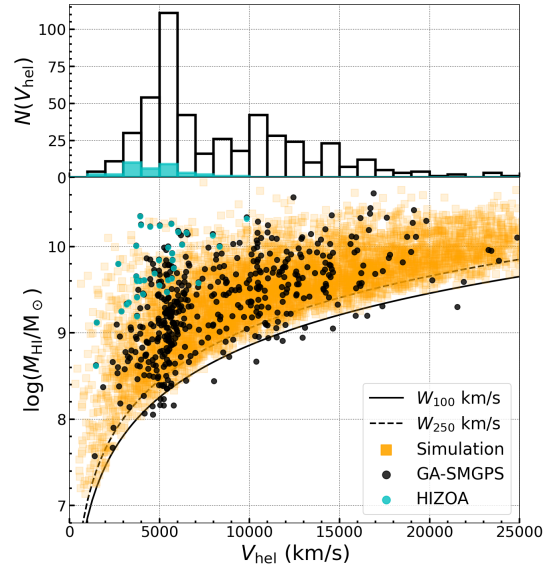


**Figure 4.** HI-masses as a function of heliocentric velocity ( $V_{\text{hel}}$ ) for the GA-SMGPS detections (black dots), with the HIZOA counterparts in cyan. The dashed and solid curves represent 5- $\sigma$  detection limits for  $W_{50}$  of 100 and 250 km s $^{-1}$ , respectively. Simulations of the full SMGPS survey area (528 deg $^2$ ) and the GA-SMGPS specifications are displayed in orange. The velocity distribution is given at the top, with HIZOA galaxies in cyan.

wiggles with high noisy spikes which might have affected the width and height determination of the profiles. The red dashed line is the result of fitting the data points (excluding the two outliers) with a linear regression least-squares fit algorithm. This routine returns a near-perfect slope of  $1.03 \pm 0.06$ , with an  $R^2$  value of 0.92 – demonstrating strong agreement between SMGPS and HIZOA fluxes. The ATCA data of the two GLIMPSE galaxies provide the only interferometric counterparts, and their agreement in flux is reassuring.

We furthermore checked consistency in positions, velocities, and linewidths. The relatively high mean angular separation of  $2.6' \pm 2.0'$  is primarily caused by HIZOA’s resolution ( $15.5'$ ). A better positional accuracy indicator is the offset with the GLIMPSE galaxies, which ranges between a mere  $6\text{--}8''$ . The shapes of the HI profiles (HIZOA vs SMGPS) are found to be very similar as well as the resulting HI parameters. The SMGPS values of  $V_{\text{sys}}$ ,  $W_{20}$  and  $W_{50}$  show no deviation from linearity compared to HIZOA. The SMGPS values have a mean error of 14, 20 and 30 km s $^{-1}$  respectively, and a standard deviation below the channel width (11, 30, 42 km s $^{-1}$ ). The HI parameters of the two GLIMPSE galaxies fall into the same range, with mean offsets of  $23$  km s $^{-1}$ ,  $12$  km s $^{-1}$  and  $15$  km s $^{-1}$ . This confirms the SMGPS calibration and HI parameters to be of good quality, well within expectations given the SMGPS channel width of 44 km s $^{-1}$ .

## 4.2 Large-Scale Structure

As a first step in our examination of the unveiled large-scale structures, as well as the HI-mass detectability of the GA-SMGPS, we display in Fig. 4 the HI-mass as a function of recessional velocity. Our detections are superimposed on a simulation that was derived following the precepts given in Staveley-Smith & Oosterloo (2015) for the SKA HI science case, tuned to the specifications of the SMGPS: 0.45 mJy rms, 44 km s $^{-1}$  channels and the full survey area of 528 deg $^2$ . The simulation assumes the HIPASS non-evolving 2D HI mass-velocity width function derived in Zwaan et al. (2005), placing galaxies at random out to the corresponding sensitivity limit of the observations. Loss of S/N ratio due to velocity width and telescope resolution are both taken into account (see also Duffy et al. 2012). These predictions are shown as orange squares, the GA-SMGPS detections as black dots, and the galaxies in common with HIZOA in cyan. The two curves represent 5- $\sigma$  detection limits for galaxies with  $W_{50} = 100$  km s $^{-1}$  (dwarfs) and 250 km s $^{-1}$  (normal spirals) for an rms of 0.45 mJy.

Figure 4 demonstrates that the HI-detections reach the limits of the 5- $\sigma$  sensitivity curves throughout the survey volume, and that we

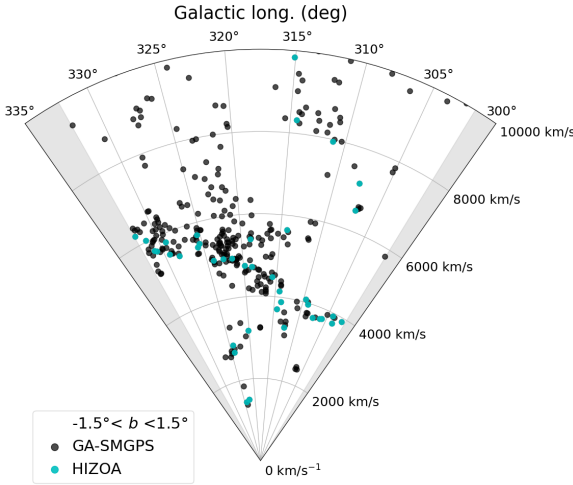


**Figure 5.** Wedge diagram of GA-SMGPS galaxy detections (black dots) and the HIZOA galaxies (cyan dots) for  $V_{\text{hel}} \leq 10000 \text{ km s}^{-1}$ .

are sensitive to  $M_{\text{HI}}^*$  galaxies out to its edge. The  $\text{H}\alpha$ -mass ranges between  $\log(M_{\text{HI}}/\text{M}_\odot) : 7.6\text{--}10.6$ . The distribution is far from uniform, revealing distinct clustering within the survey. A striking overdensity hovers around the GA distance range ( $V_{\text{hel}} \sim 5000 \text{ km s}^{-1}$ ) where it probes the gas-rich galaxy population over an order of magnitude deeper than HIZOA. The velocity histogram of this wall-like structure shows broad shoulders reaching from about 3500–6500  $\text{km s}^{-1}$  (see also Fig. 7), a typical signature of super-clusters (e.g., Kraan-Korteweg et al. 2017). Another peak around 10500  $\text{km s}^{-1}$  is not associated with any known structure. A small rise in detections around 14500  $\text{km s}^{-1}$  supports an earlier proposed connection between the rich Ara and Triangulum-Australis clusters below the Galactic plane ( $\ell, b, V = 329^\circ.3, -9^\circ.9, 14634 \text{ km s}^{-1}$  and  $324^\circ.5, -11^\circ.6, 15060 \text{ km s}^{-1}$ ; e.g., Woudt et al. 2004; Radburn-Smith et al. 2006) and the Shapley SCL (Proust et al. 2006).

#### 4.3 The GA Wall across the ZoA

To investigate the structure and morphology of the GA crossing in more detail, Fig. 5 displays the GA-SMGPS in a redshift wedge limited to  $V_{\text{hel}} < 10000 \text{ km s}^{-1}$ . The GA Wall is well-defined, starting from just below 4000  $\text{km s}^{-1}$  at the lower longitudes, up to about 6500  $\text{km s}^{-1}$  on the other side. It clearly is the dominant feature in this narrow cone. The massive HIZOA spirals (cyan dots) follow the shape outlined by the GA-SMGPS closely, but the latter shows a much denser and broader morphology with its  $\text{H}\alpha$  population of galaxies that reach well into the dwarf regime.

For more insight into the distribution of the GA connection, Fig. 6 displays an on-sky plot of the GA-SMGPS in its wider surroundings ( $295^\circ < \ell < 340^\circ; |b| < 12.5^\circ$ ) including galaxies from HIZOA ( $|b| < 5^\circ$ ), HyperLeda and the WALLABY pilot survey field in Norma (Westmeier et al. 2022). The colour coding subdivides the velocities into bins of  $\Delta V = 1000 \text{ km s}^{-1}$  over the velocity range 3500–7500  $\text{km s}^{-1}$ . The DIRBE/IRAS extinction contour (e.g., Schlafly & Finkbeiner 2011) of  $A_B = 3^{m}0$  is added to indicate where the ZoA becomes completely opaque to optical galaxies (Kraan-Korteweg & Lahav 2000; Woudt & Kraan-Korteweg 2001).

The Norma cluster at  $(\ell, b) = (325^\circ.3, -7^\circ.2)$  is the most prominent structure in Fig. 6. It appears to be the centre of a web from which a broad wall extends into the GA-SMGPS around  $\ell \sim 322^\circ$  (see green, cyan and blue dots). At the same longitude and velocity range, the

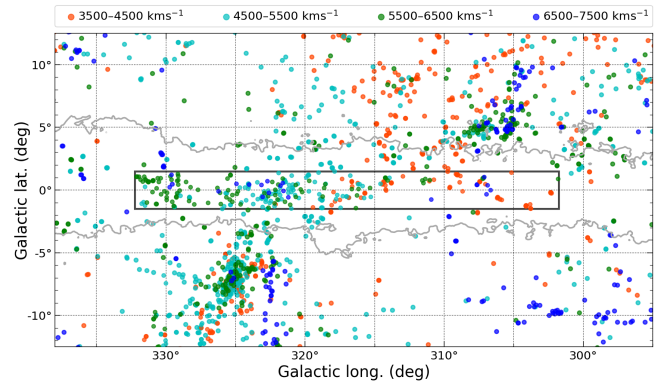


**Figure 6.** On-sky distribution of galaxies from GA-SMGPS, HIZOA, HyperLeda and WALLABY for the velocity range  $3500 < V_{\text{hel}} < 7500 \text{ km s}^{-1}$ . The black box represents the GA-SMGPS search area. The grey contour marks the  $A_B = 3^{m}0$  IRAS/DIRBE extinction level.

concentration at higher latitudes seems offset from the main GA Wall in this figure, contrary to what is seen in Fig. 5. This might suggest that the overdensity is related to a wall that connects to the Ophiuchus cluster ( $\ell, b, V \approx 0^\circ.5, 9^\circ.5, 8500 \text{ km s}^{-1}$ ; Wakamatsu et al. 2005), a hint of which had been seen in the HIZOA Galactic Bulge extension (Kraan-Korteweg et al. 2008) and also in the SMGPS LV data (Kurapatil et al. 2023). A narrow filamentary connection seems to emanate from the Norma cluster (red and green dots), extending towards the Centaurus-Crux cluster at  $306^\circ, 6^\circ, 6200 \text{ km s}^{-1}$  (Nagayama et al. 2006; Radburn-Smith et al. 2006; Koevski et al. 2007); while the red GA-SMGPS dots around  $\ell : 304^\circ - 310^\circ$  may well be associated with the PKS1343 cluster ( $309^\circ.7, 1^\circ.7, 3872 \text{ km s}^{-1}$ ; Nagayama et al. 2004; Schröder et al. 2007).

As a final step, Fig. 7 compares the GA-SMGPS velocity distribution to counts predicted by the simulation (henceforth S45) mentioned in Section 4.2. The blue histogram depicts the GA-SMGPS results, and the black solid line the S45 predictions. Note that we scaled the S45 simulations to the GA-SMGPS detection counts (not the survey area) because of the noise variations in GA-SMGPS. Although the mean rms of the mosaics (0.47 mJy) is close to the 0.45 mJy in S45, its range extends to values of 0.53 mJy. Moreover, all mosaics suffer varying degrees of noise fluctuations localised around continuum residuals. The S45 nevertheless provides a good indication of the expected counts as a function of redshift, and overall is a good representative of a more homogeneous galaxy distribution, given its nearly six times larger survey area compared to GA-SMGPS (528 deg<sup>2</sup> versus 90 deg<sup>2</sup>).

The difference between the S45 and GA-SMGPS detections highlights the enormity of the GA Wall overdensity: 45% of our detections out to 25000  $\text{km s}^{-1}$  lie within 3500–6500  $\text{km s}^{-1}$ , while S45 predict this to be around 15%, hence a factor of  $f = 3$  lower. This would imply an overdensity of  $\Delta = 2$  at the GA distance range volume. One could argue that the galaxies conforming the GA overdensity, i.e., the number of galaxies above the solid line (S45), should be subtracted when scaling S45 – to better reflect a uniform galaxy distribution in this volume. If such a re-scaling were applied (dashed line in Fig. 7), the GA Wall would obviously be even more pronounced ( $f \simeq 4.3$ , leading to an overdensity of  $\Delta \simeq 3.3$ ).

At distances beyond  $V_{\text{hel}} > 15000 \text{ km s}^{-1}$ , the counts consistently lie below the S45 curves. This could indicate lower completeness due to noise variations, which could affect the high distance range more strongly. But this is not corroborated by results obtained in other parts of the SMGPS, which show no systematic decrease at

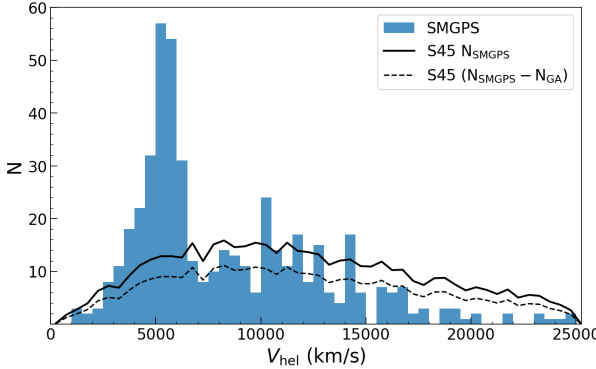


**Figure 7.** The velocity distribution of the GA-SMGPS galaxy candidates (blue histogram). The solid black gives the S45 predictions scaled to the total GA-SMGPS detections; the dashed line represents S45, *excluding* the GA-overdensity above the S45 prediction for  $3500\text{--}6500\text{ km s}^{-1}$ .

the higher redshifts. Moreover, the highest redshift detections in GA-SMGPS all lie close or even below the  $\text{H}\alpha$ -mass sensitivity curves, even the  $W_{50} = 250\text{ km s}^{-1}$  limit – a value typical for galaxies in that  $\text{H}\alpha$ -mass range. The low counts therefore seem more likely to mark a real underdensity, possibly the signature of an extended distant void.

## 5 CONCLUSIONS

The deep southern SARAO MeerKAT Galactic Plane survey ( $|b| \lesssim 1.5^\circ$ ) was analysed over an area of  $302^\circ \leq \ell \leq 332^\circ$  to chart the GA Wall across the ZoA using the 21 cm emission line of galaxies. The data comprising 157 fields were mosaicked into 10  $\text{H}\alpha$  data cubes to which the automated source finder and parameterisation algorithm SoFiA (Serra et al. 2015) was applied. Its parameter settings were optimised following a deep visual inspection of one mosaic.

Overall, 477 galaxy candidates were identified in GA-SMGPS. The considerably higher sensitivity of the SMGPS compared to HIZOA led to a substantial increase in detections: 382 versus 42 within the HIZOA volume ( $V_{\text{hel}} \leq 12000\text{ km s}^{-1}$ ). A quality assessment of the SMGPS and HIZOA found no deviations of the integrated flux over the probed flux range of  $2\text{--}30\text{ Jy km s}^{-1}$ . In view of the SMGPS channel widths ( $\sim 44\text{ km s}^{-1}$ ), the velocities and linewidths agree very well (below one channel).  $\text{H}\alpha$  detections were found down to a limit of  $\log(M_{\text{HI}}/\text{M}_\odot) = 9.8$  to the edge of the full survey volume, and down to 8.5 at the GA distance.

The structures outlined by GA-SMGPS clearly confirm the continuation of the GA Wall across the innermost ZoA. The prominence and detail of the Wall are striking: the overall galaxy counts within the velocity range  $3500\text{--}6500\text{ km s}^{-1}$  are a factor of  $f \sim 3\text{--}5$  higher compared to S45, and while the GA-SMGPS wall is wider and more densely populated, it closely follows the ‘skeleton’ structure outlined by HIZOA – consisting largely of  $\text{H}\alpha$ -massive spirals. At the largest longitudes, the Wall seems to extend to higher velocities, suggestive of a connection with the Ophiuchus SCL (e.g., Kurapati et al. 2023; Wakamatsu et al. 2005).

The highly encouraging results of the SMGPS clearly demonstrated that deep interferometric  $\text{H}\alpha$  surveys have the power to uncover the large-scale structure of galaxies, even at the lowest, most optically opaque latitudes. The deep  $\text{H}\alpha$  observations of SMGPS provide a clear view of the GA ZoA crossing: it appears as a smooth large wall-like structure with inter-connecting filaments.

Our ultimate goal is to exploit the entire SMGPS for hidden large-

scale structures. Analysis in two other dynamically important regions, the Vela SCL (Rajjohnson et al., in prep.) and the LV (Kurapati et al. 2023) are close to completion. The final papers in these series will be dedicated to a thorough completeness analysis and the derivation of the  $\text{H}\alpha$ -mass function, as well as its dependence on environment.

## ACKNOWLEDGEMENTS

We would like to thank J.M. van der Hulst and T. Westmeier for their valuable input. This research was supported by the South African Research Chairs Initiative (SARChI) of the Department of Science and Technology and National Research Foundation. The MeerKAT telescope is operated by the South African Radio Astronomy Observatory, which is a facility of the National Research Foundation, an agency of the Department of Science and Innovation. This project has received funding from the European Research Council (ERC) under the European Union’s Horizon 2020 research and innovation programme (grant agreement no. 679627).

## DATA AVAILABILITY

The full GA-SMGPS galaxy catalog is presented in Appendix B, and will be submitted to SIMBAD. Upon formal publication, the full catalog will be made available as online supplementary material, as well as an atlas of all galaxy candidates.

## REFERENCES

- Calabretta M. R., Staveley-Smith L., Barnes D. G., 2014, *Publ. Astron. Soc. Australia*, **31**, e007
- Comrie A., et al., 2021, CARTA: The Cube Analysis and Rendering Tool for Astronomy, Zenodo, doi:10.5281/zenodo.3377984
- Dressler A., Faber S. M., Burstein D., Davies R. L., Lynden-Bell D., Terlevich R. J., Wegner G., 1987, *ApJ*, **313**, L37
- Duffy A. R., Meyer M. J., Staveley-Smith L., Bernyk M., Croton D. J., Koribalski B. S., Gerstmann D., Westerlund S., 2012, *MNRAS*, **426**, 3385
- Henning P. A., 1992, *ApJS*, **78**, 365
- Jarrett T. H., et al., 2007, *AJ*, **133**, 979
- Józsa G. I. G., et al., 2020, arXiv e-prints, p. arXiv:2006.02955
- Kocevski D. D., Ebeling H., Mullis C. R., Tully R. B., 2007, *ApJ*, **662**, 224
- Koribalski B. S., et al., 2020, *Ap&SS*, **365**, 118
- Kraan-Korteweg R. C., Lahav O., 2000, *A&ARv*, **10**, 211
- Kraan-Korteweg R. C., Woudt P. A., Cayatte V., Fairall A. P., Balkowski C., Henning P. A., 1996, *Nature*, **379**, 519
- Kraan-Korteweg R. C., Shafi N., Koribalski B. S., Staveley-Smith L., Buckland P., Henning P. A., Fairall A. P., 2008, in Galaxies in the Local Volume. p. 13 (arXiv:0710.1795), doi:J47-52578
- Kraan-Korteweg R. C., Cluver M. E., Bilicki M., Jarrett T. H., Colless M., Elagali A., Böhringer H., Chon G., 2017, *MNRAS*, **466**, L29
- Kurapati S., et al., 2023, MNRAS (submitted), Manuscript ID: MN-23-4456-MJ
- Lynden-Bell D., Faber S. M., Burstein D., Davies R. L., Dressler A., Terlevich R. J., Wegner G., 1988, *ApJ*, **326**, 19
- Makhathini S., 2018, PhD thesis, Rhodes University, South Africa
- Mauch T., et al., 2020, *ApJ*, **888**, 61
- Nagayama T., et al., 2004, *MNRAS*, **354**, 980
- Nagayama T., et al., 2006, *MNRAS*, **368**, 534
- Proust D., et al., 2006, *A&A*, **447**, 133
- Radburn-Smith D. J., Lucey J. R., Woudt P. A., Kraan-Korteweg R. C., Watson F. G., 2006, *MNRAS*, **369**, 1131
- Ramatsoku M., et al., 2016, *MNRAS*, **460**, 923

- Schlafly E. F., Finkbeiner D. P., 2011, [ApJ, 737, 103](#)
- Schröder A. C., Mamon G. A., Kraan-Korteweg R. C., Woudt P. A., 2007, [A&A, 466, 481](#)
- Scrimgeour M. I., et al., 2016, [MNRAS, 455, 386](#)
- Serra P., et al., 2015, [MNRAS, 448, 1922](#)
- Springob C. M., et al., 2016, [MNRAS, 456, 1886](#)
- Staveley-Smith L., Oosterloo T., 2015, in Advancing Astrophysics with the Square Kilometre Array (AASKA14). p. 167 ([arXiv:1506.04473](#))
- Staveley-Smith L., et al., 1998, [AJ, 116, 2717](#)
- Staveley-Smith L., Kraan-Korteweg R. C., Schröder A. C., Henning P. A., Koribalski B. S., Stewart I. M., Heald G., 2016, [AJ, 151, 52](#)
- Steyn N., 2023, Master's thesis, University of Cape Town, South Africa, <https://open.uct.ac.za/handle/11427/38045>
- Tully R. B., Pomarède D., Graziani R., Courtois H. M., Hoffman Y., Shaya E. J., 2019, [ApJ, 880, 24](#)
- Wakamatsu K., Malkan M. A., Nishida M. T., Parker Q. A., Saunders W., Watson F. G., 2005, in Fairall A. P., Woudt P. A., eds, Astronomical Society of the Pacific Conference Series Vol. 329, Nearby Large-Scale Structures and the Zone of Avoidance. p. 189
- Wang J., Koribalski B. S., Serra P., van der Hulst T., Roychowdhury S., Kamphuis P., Chengalur J. N., 2016, [MNRAS, 460, 2143](#)
- Westmeier T., et al., 2021, [MNRAS, 506, 3962](#)
- Westmeier T., et al., 2022, [Publ. Astron. Soc. Australia, 39, e058](#)
- Woudt P. A., Kraan-Korteweg R. C., 2001, [A&A, 380, 441](#)
- Woudt P. A., Kraan-Korteweg R. C., Cayatte V., Balkowski C., Felenbok P., 2004, [A&A, 415, 9](#)
- Woudt P. A., Kraan-Korteweg R. C., Lucey J., Fairall A. P., Moore S. A. W., 2008, [MNRAS, 383, 445](#)
- Zwaan M. A., Meyer M. J., Staveley-Smith L., Webster R. L., 2005, [MNRAS, 359, L30](#)

**APPENDIX A****SoFiA v2.3.1 Parameter Settings**

```

# Global settings
pipeline.verbose = false
pipeline.pedantic = false

# Input
input.data = /idia/projects/vela/V1_GA_CARACal/output_T19/mosaics/T19_gal.fits
input.region = 1457,5659,355,3959,9,570 #square region of 3x3 deg (slightly different for different mosaics)
input.gain =
input.noise = /idia/projects/vela/V1_GA_CARACal/output_T19/mosaics/T19_gal_noise.fits
input.weights =
input.mask =
input.invert = false

# Flagging
flag.region =
flag.auto = false
flag.threshold = 5.0
flag.log = true

# Noise scaling
scaleNoise.enable = true
scaleNoise.mode = spectral
scaleNoise.gridXY = 0
scaleNoise.gridZ = 0
scaleNoise.interpolate = false
scaleNoise.scfind = true # normalises the noise after each S+C smoothing step

# S+C finder (smooth & clip)
scfind.enable = true
scfind.kernelsXY = 0, 10, 20, 30
scfind.kernelsZ = 0, 3, 7
scfind.threshold = 3.5 #4.0
scfind.replacement = 1.5
scfind.statistic = mad
scfind.fluxRange = negative

# Linker
linker.radiusXY = 5
linker.radiusZ = 1
linker.minSizeXY = 8
linker.minSizeZ = 2
linker.maxSizeXY = 0
linker.maxSizeZ = 21 #31

# Reliability
reliability.enable = true
reliability.threshold = 0.70
reliability.scaleKernel = 0.25 # Sofia 2.4.0 will use the auto-kernel feature if set to 0
reliability.minSNR = 3 # Replaced reliability.fmin in latest Sofia2 update
reliability.plot = true
reliability.debug = true

# Parameterisation
parameter.enable = true
parameter.wcs = true
parameter.physical = true
parameter.prefix = SoFiA
parameter.offset = true # The position parameters will be relative to the full cube (when specifying input.region)

```

```
# Output
output.directory = /users/nadia/Sofia2/
output.filename = T19
output.writeCatASCII = true
output.writeCatXML = false
output.writeCatSQL = false
output.writeNoise = false
output.writeFiltered = false
output.writeMask = false
output.writeMask2d = false
output.writeMoments = false
output.writeCubelets = false
output.marginCubelets = 0
output.overwrite = true
```

**APPENDIX B****The SARA MeerKAT Galactic Plane Survey: Full Catalog (GA region)**

A brief description of the parameters follows. Parameters are given by SoFiA unless otherwise stated.

- (1) SMGPS identifier, reflecting the equatorial coordinates [SMGPS-HI-Jhhmmss  $\pm$  ddmmss].
- (2) Mosaic name [T10–T19].
- (3) Galactic longitude [deg].
- (4) Galactic latitude [deg].
- (5) Peak flux density – taken from the HI profile [Jy].
- (6) Integrated flux [ $\text{Jy km s}^{-1}$  ].
- (7) Integrated flux error – measured in emission-free areas surrounding the source [ $\text{Jy km s}^{-1}$  ].
- (8) Local rms – as measured in the corners of the sub-cube [ $\text{Jy beam}^{-1}$  ].
- (9) Heliocentric velocity (optical convention) [ $\text{km s}^{-1}$  ].
- (10) Line width at 20% of the peak flux density, measured in the observer’s frame [ $\text{km s}^{-1}$  ].
- (11) Line width at 50% of the peak flux density, measured in the observer’s frame [ $\text{km s}^{-1}$  ].
- (12) HI mass [ $\log M_{\odot}$ ], calculated as follows:

$$M_{\text{HI}} = \frac{2.356 \times 10^5}{1+z} D^2 S_{\text{int}},$$

where  $D$  is the approximate luminosity distance in Mpc, calculated by  $D = \frac{V_{\text{hel}}}{H_0}$ , where  $H_0$  is taken as  $70 \text{ km s}^{-1} \text{ Mpc}^{-1}$ . Note HI masses have not been corrected to the barycentre of the Local Group ( $V_{\text{LG}}$ ), nor corrected for the limited instrumental resolution.

- (13) Flag – category 1 (high confidence) or 2 (slightly lower confidence).
- (14) Note – Comment, or name of counterpart. Names starting with ‘J’ are HIZOA names. Note, names from earlier HIZOA publications (e.g., HIPASS, HIZSS) and dedicated follow-up observations are omitted.

Footnotes are found at the end of the table.

**The GA-SMGPS galaxy catalog.**

SMGPS name J2000 (1)	Mosaic TXX (2)	$\ell$ deg (3)	$b$ deg (4)	$S_{\text{peak}}$ Jy (5)	$S_{\text{int}}$ Jy km/s (6)	$\text{err}_{S_{\text{int}}}$ Jy km/s (7)	RMS Jy km/s (8)	$V_{\text{hel}}$ km/s (9)	$W_{20}$ km/s (10)	$W_{50}$ km/s (11)	$\log M_{\text{HI}}$ $\log M_{\odot}$ (12)	Flag 1/2 (13)	Note or counterpart
J124141-620158	T19	301.788	0.817	0.008	1.25	0.18	0.33	12051	228	212	9.93	1	
J124160-615621	T19	301.821	0.912	0.008	0.46	0.09	0.33	5817	116	82	8.87	1	
J124342-620018	T19	302.024	0.853	0.005	0.42	0.06	0.29	12042	277	277	9.45	1	
J124404-624235	T19	302.088	0.150	0.006	0.94	0.13	0.26	10920	267	225	9.72	1	
J124431-622415	T19	302.130	0.457	0.010	0.78	0.11	0.29	11780	138	82	9.70	1	
J124532-624150	T19	302.255	0.167	0.010	0.84	0.12	0.26	11828	126	97	9.73	1	
J124624-630308	T19	302.362	-0.186	0.093	30.84	3.04	0.35	3912	489	455	10.35	1	J1246-63, IRAS 12362-5919
J124734-630933	T19	302.494	-0.291	0.012	1.66	0.24	0.28	10105	266	241	9.90	1	
J124738-640005	T19	302.514	-1.133	0.007	0.68	0.10	0.34	10026	183	183	9.50	1	
J124844-621629	T19	302.618	0.595	0.012	1.95	0.19	0.33	11492	276	248	10.08	1	
J125027-620604	T19	302.816	0.770	0.007	0.92	0.09	0.30	15601	365	341	10.01	2	
J125060-614758	T19	302.880	1.072	0.018	1.12	0.11	0.36	15657	114	75	10.10	1	
J125146-622743	T19	302.970	0.410	0.004	0.51	0.07	0.30	11786	353	328	9.52	1	
J125214-632227	T19	303.021	-0.503	0.007	0.95	0.13	0.25	12876	225	210	9.86	1	
J125248-630837	T19	303.085	-0.272	0.006	0.63	0.09	0.24	12537	231	221	9.66	1	
J125255-631242	T19	303.099	-0.340	0.005	0.68	0.10	0.26	12587	323	292	9.70	1	
J125400-625346	T19	303.224	-0.026	0.002	0.11	0.02	0.23	12934	133	108	8.94	1	
J125446-640154	T19	303.296	-1.162	0.007	0.31	0.04	0.30	10116	92	76	9.17	1	
J125500-630545	T19	303.335	-0.227	0.009	0.97	0.14	0.27	10071	183	183	9.66	1	
J125625-631226	T19	303.493	-0.341	0.006	1.05	0.10	0.27	15920	326	302	10.09	1	
J125701-624842	T19	303.568	0.053	0.010	1.60	0.16	0.30	12929	259	225	10.09	1	

## GA-SMGPS galaxy catalog –Continued.

SMGPS name J2000 (1)	Mosaic TXX (2)	$\ell$ deg (3)	$b$ deg (4)	$S_{\text{peak}}$ Jy (5)	$S_{\text{int}}$ Jy km/s (6)	$\text{err}_{S_{\text{int}}}$ Jy km/s (7)	RMS Jy km/s (8)	$V_{\text{hel}}$ km/s (9)	$W_{20}$ km/s (10)	$W_{50}$ km/s (11)	$\log M_{\text{HI}}$ $\log M_{\odot}$ (12)	Flag 1/2 (13)	Note or counterpart
J125729-625317	T19	303.621	-0.025	0.004	0.27	0.04	0.27	15910	137	121	9.50	1	
J125841-620529	T19	303.780	0.768	0.011	0.81	0.12	0.32	9844	86	71	9.56	1	
J125907-641822	T19	303.765	-1.447	0.025	3.86	0.55	0.71	3756	215	200	9.41	1 J1259-64	
J125932-635841	T19	303.819	-1.120	0.014	1.33	0.25	0.34	3912	135	117	8.99	1	
J125937-624059	T19	303.870	0.174	0.009	0.65	0.09	0.30	10535	128	109	9.52	1	
J130033-625813	T19	303.967	-0.117	0.007	0.47	0.07	0.27	10105	127	112	9.35	1	
J130211-640338	T19	304.107	-1.213	0.017	2.64	0.37	0.37	3917	253	223	9.28	1 J1302-64 B, 2MASS J13021348-6403556	
J130219-621523	T19	304.197	0.589	0.009	1.19	0.12	0.36	13789	311	133	10.02	1	
J130235-640621	T19	304.148	-1.260	0.021	1.61	0.23	0.36	3923	157	101	9.07	1 J1302-64 A	
J130247-614827	T19	304.272	1.035	0.007	0.95	0.13	0.35	13738	330	280	9.92	1	
J130804-622610	T18	304.855	0.373	0.006	0.13	0.02	0.43	15894	83	53	9.18	2	
J130804-625122	T18	304.827	-0.046	0.007	1.05	0.10	0.44	19820	414	329	10.27	2	
J130833-630248	T18	304.870	-0.239	0.007	1.01	0.14	0.48	12131	231	231	9.84	1	
J130932-640405	T18	304.908	-1.266	0.015	1.17	0.12	0.52	16626	421	161	10.17	2 group <sup>1</sup>	
J131002-612302	T18	305.157	1.408	0.012	0.56	0.10	0.43	3904	45	45	8.61	1	
J131053-635201	T19	305.071	-1.076	0.005	0.23	0.03	0.37	12271	92	86	9.21	2	
J131127-634643	T18	305.141	-0.993	0.010	1.17	0.17	0.39	7822	270	254	9.53	1	
J131202-634757	T18	305.204	-1.018	0.024	3.41	0.48	0.41	7711	220	170	9.98	1	
J131319-631846	T18	305.386	-0.545	0.005	0.51	0.07	0.44	12136	171	138	9.54	1	
J131435-632335	T18	305.521	-0.638	0.008	1.12	0.16	0.43	12298	442	359	9.89	2	
J131744-633015	T18	305.861	-0.782	0.055	2.33	0.33	0.45	3750	72	45	9.19	1 J1318-63	
J131924-635630	T18	305.997	-1.236	0.014	1.22	0.17	0.42	12729	225	188	9.96	1	
J132005-631728	T18	306.145	-0.598	0.006	0.43	0.04	0.32	24852	231	145	10.07	2	
J132011-631618	T18	306.157	-0.580	0.036	6.03	0.86	0.46	3743	236	151	9.60	1 J1320-63	
J132158-621724	T18	306.473	0.372	0.010	0.34	0.05	0.34	9690	46	29	9.18	1	
J132322-620858	T18	306.651	0.491	0.006	0.18	0.06	0.32	2392	36	22	7.68	2	
J132407-623712	T18	306.679	0.014	0.010	3.05	0.43	0.38	6609	492	456	9.80	1	
J132532-621306	T18	306.894	0.391	0.008	1.16	0.16	0.35	6567	453	450	9.37	1	
J132642-613202	T18	307.121	1.051	0.029	7.29	0.72	0.35	6503	307	287	10.16	1 J1327-61	
J132652-620544	T18	307.065	0.491	0.020	1.28	0.24	0.35	3733	45	45	8.93	1	
J132659-625456	T18	306.965	-0.322	0.014	0.96	0.14	0.34	6609	121	84	9.30	1	
J132836-632540	T18	307.074	-0.855	0.009	0.28	0.09	0.31	2437	36	22	7.90	2	
J132934-635331	T18	307.112	-1.330	0.033	1.69	0.31	0.46	2383	81	54	8.66	1	
J133002-615146	T18	307.465	0.669	0.087	15.63	1.54	0.39	3696	253	222	10.01	1 J1329-61	
J133202-620407	T18	307.667	0.429	0.028	1.57	0.22	0.36	7152	88	55	9.58	1 J1331-62	
J133415-631618	T18	307.724	-0.799	0.005	0.47	0.07	0.28	12709	185	167	9.54	1	
J133736-631519	T18	308.098	-0.847	0.007	0.48	0.07	0.25	9932	92	80	9.35	1	
J134019-615716	T17	308.643	0.374	0.023	2.03	0.29	0.53	7516	91	88	9.73	1	
J134043-610942	T17	308.841	1.143	0.012	1.39	0.26	0.55	3672	193	130	8.95	1	
J134129-622316	T17	308.694	-0.077	0.010	0.43	0.08	0.42	3767	45	45	8.46	1	
J134158-613945	T17	308.890	0.623	0.010	0.61	0.11	0.44	3772	129	81	8.62	1	
J134227-610114	T17	309.072	1.242	0.076	23.92	2.36	0.72	3964	391	326	10.25	1 J1342-61, DZOA 4649-06 <sup>2</sup>	
J134309-605759	T17	309.167	1.278	0.021	0.87	0.16	0.60	4030	73	46	8.83	2	
J134319-625119	T17	308.810	-0.577	0.008	0.60	0.09	0.28	12642	92	92	9.64	1	
J134831-605751	T17	309.804	1.144	0.012	1.45	0.14	0.64	17605	250	104	10.31	2	
J134849-615619	T17	309.625	0.185	0.054	3.61	0.51	0.54	4073	108	65	9.45	1 J1348-61	
J135335-610333	T17	310.380	0.911	0.017	1.80	0.26	0.55	8005	168	130	9.73	2	
J135639-610312	T17	310.741	0.826	0.025	4.55	0.65	0.47	3811	223	181	9.50	1	
J135753-610405	T16	310.883	0.774	0.015	2.42	0.34	0.45	8449	390	343	9.91	2	
J135831-610248	T16	310.962	0.775	0.010	1.70	0.24	0.38	8565	274	239	9.77	1	
J135911-605931	T16	311.054	0.807	0.014	1.02	0.14	0.35	5915	90	73	9.23	1	
J135922-611215	T16	311.020	0.596	0.010	0.91	0.13	0.41	8014	176	158	9.44	1	
J135930-610330	T16	311.074	0.733	0.010	0.65	0.12	0.40	3971	90	81	8.68	1	
J140130-604917	T16	311.371	0.897	0.008	0.59	0.11	0.37	5501	90	78	8.93	1	
J140144-623126	T16	310.940	-0.750	0.012	1.39	0.20	0.44	7137	136	136	9.52	1	

## GA-SMGPS galaxy catalog –Continued.

SMGPS name J2000 (1)	Mosaic TXX (2)	$\ell$ deg (3)	$b$ deg (4)	$S_{\text{peak}}$ Jy (5)	$S_{\text{int}}$ Jy km/s (6)	$\text{err}_{S_{\text{int}}}$ Jy km/s (7)	RMS Jy km/s (8)	$V_{\text{hel}}$ km/s (9)	$W_{20}$ km/s (10)	$W_{50}$ km/s (11)	$\log M_{\text{HI}}$ $\log M_{\odot}$ (12)	Flag 1/2 (13)	Note or counterpart
J140147-615220	T16	311.121	-0.124	0.008	0.86	0.12	0.53	9968	280	216	9.60	2	
J140259-602854	T16	311.637	1.175	0.008	0.80	0.11	0.55	9394	320	320	9.52	1	
J140316-605941	T16	311.530	0.672	0.007	1.06	0.15	0.39	8741	228	202	9.58	1	
J140320-610558	T16	311.509	0.569	0.008	0.57	0.10	0.40	5529	135	74	8.91	1	
J140325-605235	T16	311.581	0.781	0.009	0.65	0.09	0.40	5933	136	112	9.03	1	
J140413-603211	T16	311.769	1.081	0.010	0.72	0.10	0.43	8145	182	182	9.35	1	
J140445-631057	T16	311.090	-1.478	0.021	4.61	0.45	0.96	7951	273	273	10.13	1	
J140449-612305	T16	311.601	0.246	0.006	0.73	0.07	0.46	19228	215	178	10.08	1	
J140454-611442	T16	311.649	0.377	0.017	1.73	0.25	0.48	8339	171	148	9.75	1	
J140537-601402	T16	312.019	1.322	0.009	0.74	0.11	0.46	9427	183	164	9.49	1	
J140614-603014	T16	312.016	1.042	0.009	0.74	0.11	0.34	11022	223	196	9.62	1	
J140620-603229	T16	312.016	1.003	0.005	0.27	0.04	0.30	11538	92	74	9.22	1	
J140807-603938	T16	312.192	0.825	0.005	0.49	0.07	0.35	14623	232	214	9.68	1	
J141057-602613	T16	312.591	0.935	0.011	0.62	0.09	0.36	14418	85	70	9.77	1	
J141151-613818	T16	312.328	-0.242	0.007	0.91	0.13	0.46	11349	300	227	9.74	1	
J141224-612258	T16	312.470	-0.019	0.006	0.56	0.08	0.47	14177	232	232	9.71	1	
J141249-621625	T16	312.242	-0.882	0.013	1.30	0.24	0.46	3102	169	147	8.78	1	
J141330-612227	T16	312.597	-0.052	0.010	0.46	0.07	0.44	8386	46	46	9.18	1	
J141333-600959	T16	312.980	1.094	0.011	0.94	0.17	0.33	3657	90	90	8.77	1	
J141425-605213	T16	312.861	0.392	0.010	0.82	0.12	0.43	11279	184	160	9.68	1	
J141426-600124	T16	313.129	1.195	0.012	0.55	0.08	0.36	13632	46	46	9.67	1	
J141427-622556	T16	312.372	-1.092	0.019	0.96	0.18	0.51	3352	84	68	8.71	1	
J141435-612420	T16	312.712	-0.123	0.016	2.23	0.32	0.50	8134	291	195	9.84	2	
J141442-613654	T16	312.659	-0.326	0.010	1.10	0.16	0.48	11531	248	168	9.83	2	
J141503-603143	T16	313.043	0.691	0.016	3.04	0.30	0.37	11017	554	417	10.23	1	
J141503-610757	T16	312.850	0.119	0.013	1.55	0.15	0.43	12876	247	150	10.07	1	
J141521-621113	T16	312.548	-0.892	0.027	4.34	0.61	0.50	3285	204	174	9.35	1	
J141557-623832 T16 312.469 -1.346 0.026 1.10 0.20 0.80 3445 45 39 8.79 1													
J141652-615941	T16	312.779	-0.767	0.009	0.79	0.11	0.41	8562	159	120	9.43	1	
J141835-612830	T16	313.141	-0.343	0.006	0.12	0.02	0.37	11832	289	210	8.90	2	
J141846-603302	T16	313.467	0.523	0.007	0.48	0.07	0.30	10056	183	155	9.36	1	
J141931-601920	T16	313.630	0.707	0.017	1.45	0.21	0.33	10636	92	92	9.88	1	
J142001-594727	T15	313.867	1.187	0.007	0.46	0.07	0.36	10489	92	92	9.37	1	
J142103-595703	T15	313.936	0.993	0.013	1.45	0.21	0.31	5302	180	155	9.29	1	
J142109-595153	T15	313.977	1.069	0.007	0.14	0.02	0.27	17381	84	52	9.28	1	
J142111-600236	T15	313.920	0.900	0.005	0.23	0.03	0.27	10859	92	92	9.10	1	
J142120-602328	T15	313.820	0.566	0.028	5.57	0.79	0.36	3891	269	269	9.60	1	
J142139-604552 T16 313.729 0.202 0.006 0.44 0.06 0.30 14493 186 186 9.63 1 J1421-60													
J142209-614849	T16	313.425	-0.804	0.027	1.94	0.28	0.40	3423	90	76	9.03	1	
J142239-600634	T15	314.070	0.775	0.016	0.99	0.14	0.32	5604	45	45	9.17	1	
J142320-595138	T15	314.236	0.979	0.040	12.00	1.18	0.36	5650	565	529	10.26	1	
J142345-600756	T15	314.190	0.706	0.004	0.36	0.05	0.27	17388	375	359	9.69	2	
J142357-602412	T15	314.118	0.444	0.019	1.28	0.18	0.40	8487	121	88	9.64	1	
J142415-603101	T15	314.113	0.324	0.006	0.60	0.09	0.30	14488	269	224	9.76	1	
J142446-603711	T15	314.137	0.205	0.010	0.63	0.09	0.34	10589	127	111	9.52	1	
J142448-594049	T15	314.471	1.084	0.018	3.06	0.30	0.40	8326	273	273	10.00	1	
J142504-602434	T15	314.246	0.389	0.013	0.50	0.09	0.33	4390	37	23	8.66	2	
J142510-600550	T15	314.367	0.677	0.032	4.96	0.70	0.33	4142	222	198	9.61	1	
J142547-605013	T15	314.176	-0.042	0.011	0.91	0.17	0.34	4286	90	84	8.90	1	
J142551-604323	T15	314.223	0.062	0.029	2.24	0.32	0.38	4314	127	89	9.30	1	
J142554-602916	T15	314.313	0.280	0.007	0.17	0.03	0.32	8525	46	46	8.77	1	
J142600-614812	T15	313.855	-0.954	0.008	1.15	0.16	0.36	8659	274	259	9.60	1	
J142621-601356	T15	314.458	0.498	0.037	6.82	0.97	0.34	3711	224	213	9.65	1	
J142720-600942	T15	314.597	0.520	0.008	0.81	0.11	0.28	5457	135	121	9.05	1	
J142739-612022	T15	314.206	-0.592	0.010	1.20	0.17	0.31	8252	228	195	9.58	1	

## GA-SMGPS galaxy catalog –Continued.

SMGPS name J2000 (1)	Mosaic TXX (2)	$\ell$ deg (3)	$b$ deg (4)	$S_{\text{peak}}$ Jy (5)	$S_{\text{int}}$ Jy km/s (6)	$\text{err}_{S_{\text{int}}}$ Jy km/s (7)	RMS Jy km/s (8)	$V_{\text{hel}}$ km/s (9)	$W_{20}$ km/s (10)	$W_{50}$ km/s (11)	$\log M_{\text{HI}}$ $\log M_{\odot}$ (12)	Flag 1/2 (13)	Note or counterpart
J142845-611259	T15	314.373	-0.525	0.017	1.78	0.25	0.34	9304	183	183	9.86	1	
J142934-613043	T15	314.356	-0.836	0.004	0.26	0.04	0.28	14411	325	325	9.39	1	
J143036-610716	T15	314.616	-0.519	0.007	0.40	0.06	0.32	9037	109	69	9.19	2	
J143042-605733	T15	314.688	-0.373	0.011	1.34	0.19	0.34	10464	265	249	9.83	1	
J143107-611941	T15	314.596	-0.735	0.011	1.51	0.15	0.31	19118	283	268	10.40	1	
J143131-611207	T15	314.689	-0.636	0.014	2.59	0.26	0.31	9448	274	274	10.03	1	
J143313-604541	T15	315.047	-0.306	0.010	0.30	0.04	0.30	10485	83	52	9.19	1	
J143327-594404	T15	315.466	0.631	0.007	0.43	0.06	0.30	8346	137	137	9.15	1	
J143328-611930	T15	314.859	-0.839	0.004	0.11	0.02	0.26	14630	93	76	9.04	1	
J143332-610746	T15	314.941	-0.661	0.010	0.50	0.07	0.29	18958	47	47	9.91	1	
J143347-601128	T15	315.329	0.194	0.005	0.30	0.06	0.32	5534	181	181	8.64	1	
J143427-594240	T15	315.592	0.604	0.007	0.54	0.08	0.28	12743	92	92	9.61	1	
J143505-611315	T15	315.077	-0.817	0.033	4.68	0.46	0.34	9839	179	164	10.32	1 J1435-61	
J143520-585617	T15	315.995	1.273	0.006	0.34	0.05	0.34	14096	128	112	9.49	1	
J143551-605214	T15	315.299	-0.531	0.015	1.30	0.18	0.32	4525	155	107	9.10	1	
J143725-595045	T15	315.881	0.335	0.004	0.12	0.02	0.29	5035	82	52	8.15	2	
J143759-602533	T15	315.716	-0.226	0.078	17.88	1.76	0.42	4471	341	305	10.23	1 J1437-60	
J143826-593730	T15	316.087	0.486	0.006	0.21	0.04	0.33	4954	90	66	8.40	1	
J143911-592916	T15	316.230	0.573	0.009	0.34	0.06	0.35	4434	110	60	8.51	1	
J143913-593419	T15	316.200	0.494	0.005	0.16	0.03	0.30	5418	123	83	8.35	1	
J143940-604606	T15	315.766	-0.622	0.018	0.84	0.16	0.34	4582	82	59	8.92	1	
J144023-595745	T15	316.175	0.078	0.007	0.16	0.03	0.35	5632	75	47	8.38	2	
J144108-584315	T14	316.770	1.172	0.012	3.32	0.47	0.50	4963	525	497	9.59	1	
J144110-603922	T15	315.980	-0.595	0.010	0.42	0.08	0.32	4362	45	45	8.58	1	
J144119-594648	T15	316.357	0.197	0.016	2.71	0.27	0.44	9088	294	244	10.02	1	
J144151-591331	T15	316.646	0.675	0.015	1.47	0.21	0.40	4066	176	132	9.06	1	
J144153-591231	T15	316.657	0.688	0.022	3.40	0.48	0.43	4116	334	245	9.44	2 two galaxies?	
J144155-591056	T15	316.672	0.710	0.012	0.63	0.12	0.38	4218	124	87	8.73	1	
J144210-605933	T15	315.953	-0.952	0.007	0.98	0.14	0.35	10553	448	428	9.71	1	
J144228-602503	T15	316.224	-0.443	0.015	2.32	0.23	0.40	10643	267	253	10.09	1	
J144236-582527	T14	317.067	1.363	0.010	0.22	0.03	0.46	10908	46	29	9.08	2	
J144249-602252	T15	316.279	-0.428	0.010	1.39	0.20	0.40	5610	216	176	9.31	1	
J144254-593444	T15	316.622	0.297	0.005	0.39	0.07	0.38	4155	160	124	8.50	2	
J144308-595142	T15	316.531	0.028	0.005	0.36	0.05	0.39	14256	223	185	9.52	2	
J144321-593460	T15	316.672	0.270	0.003	0.14	0.02	0.34	13078	93	93	9.05	2	
J144349-594514	T15	316.653	0.090	0.006	0.31	0.06	0.41	5523	90	84	8.66	1	
J144423-610551	T15	316.154	-1.159	0.011	0.61	0.09	0.36	10476	92	77	9.49	1	
J144608-584238	T14	317.364	0.910	0.008	0.23	0.04	0.35	4112	38	24	8.27	2	
J144643-602239	T15	316.718	-0.629	0.004	0.40	0.06	0.36	18503	217	185	9.79	2	
J144656-591332	T14	317.237	0.400	0.014	2.08	0.21	0.46	11231	304	148	10.09	1 two sources?	
J144659-611545	T15	316.367	-1.442	0.015	0.83	0.12	0.74	5766	176	142	9.12	1	
J144745-601709	T14	316.872	-0.601	0.024	7.31	1.04	0.43	4484	397	383	9.84	1 GLIMPSE2, WISEA J144744.97-601704.0	
J144758-575741	T14	317.903	1.483	0.011	0.30	0.06	0.60	4647	45	45	8.49	1	
J144835-605320	T15	316.703	-1.189	0.009	0.83	0.12	0.42	14071	325	288	9.88	1	
J144837-600719	T14	317.040	-0.500	0.017	3.70	0.52	0.40	4542	427	381	9.56	1 GLIMPSE1	
J145003-591445	T14	317.587	0.208	0.018	0.93	0.17	0.43	3244	110	62	8.67	2	
J145028-600005	T14	317.301	-0.493	0.020	5.06	0.72	0.39	5361	442	423	9.84	1	
J145043-591550	T14	317.656	0.154	0.014	1.06	0.20	0.39	3240	90	85	8.72	1	
J145116-604726	T14	317.040	-1.244	0.008	0.34	0.05	0.34	11828	122	92	9.34	1	
J145135-594435	T14	317.540	-0.323	0.003	0.21	0.03	0.33	11001	225	201	9.07	1	
J145227-592145	T14	317.808	-0.032	0.004	0.15	0.03	0.35	11031	46	46	8.93	2	
J145255-600846	T14	317.510	-0.759	0.038	8.32	1.18	0.39	4288	261	239	9.86	1	
J145258-594260	T14	317.708	-0.378	0.004	0.11	0.02	0.32	4636	45	45	8.05	1	
J145326-592834	T14	317.869	-0.190	0.007	0.34	0.05	0.38	11026	184	173	9.29	1	
J145407-592406	T14	317.980	-0.162	0.009	0.65	0.12	0.38	4255	134	104	8.75	1	

## GA-SMGPS galaxy catalog –Continued.

SMGPS name J2000 (1)	Mosaic TXX (2)	$\ell$ deg (3)	$b$ deg (4)	$S_{\text{peak}}$ Jy (5)	$S_{\text{int}}$ Jy km/s (6)	$\text{err}_{S_{\text{int}}}$ Jy km/s (7)	RMS Jy km/s (8)	$V_{\text{hel}}$ km/s (9)	$W_{20}$ km/s (10)	$W_{50}$ km/s (11)	$\log M_{\text{HI}}$ $\log M_{\odot}$ (12)	Flag 1/2 (13)	Note or counterpart
J145445-595906	T14	317.787	-0.719	0.005	0.44	0.08	0.32	5420	354	339	8.79	1	
J145451-604438	T14	317.452	-1.400	0.021	1.84	0.26	0.76	5249	180	180	9.38	1	
J145532-583339	T14	318.527	0.502	0.036	5.04	0.71	0.35	4706	298	101	9.72	1	
J145540-582735	T14	318.589	0.584	0.008	0.73	0.10	0.33	11627	220	188	9.66	1	
J145551-573053	T14	319.045	1.412	0.010	0.70	0.13	0.54	4880	169	77	8.90	1	
J145552-583350	T14	318.565	0.479	0.011	0.76	0.11	0.34	5970	45	45	9.10	1	
J145558-600531	T14	317.873	-0.883	0.054	4.41	0.63	0.35	4468	122	86	9.62	1	
J145617-574540	T14	318.983	1.166	0.008	0.25	0.04	0.33	23852	86	69	9.79	1	
J145725-584745	T14	318.635	0.181	0.014	1.46	0.21	0.34	6351	136	119	9.44	1	
J145731-593252	T14	318.297	-0.491	0.007	0.71	0.10	0.31	15824	233	210	9.91	1	
J145846-601546	T14	318.102	-1.196	0.009	0.84	0.16	0.39	4366	135	135	8.88	1	
J145853-582347	T14	318.991	0.444	0.007	0.31	0.04	0.32	13320	231	84	9.41	1	
J145945-584317	T14	318.937	0.105	0.011	0.35	0.05	0.33	23263	48	35	9.93	2	
J145949-581438	T14	319.171	0.521	0.023	1.29	0.13	0.36	13962	86	71	10.06	1	
J150020-580251	T14	319.324	0.662	0.012	1.16	0.16	0.35	4649	168	93	9.08	1	
J150048-592024	T14	318.763	-0.504	0.008	0.70	0.10	0.33	5545	111	81	9.01	1	
J150115-572336	T13	319.744	1.179	0.020	6.10	0.87	0.50	4629	474	425	9.79	1	
J150138-593023	T14	318.777	-0.701	0.005	0.16	0.03	0.28	5411	134	118	8.36	1	
J150145-590347	T14	319.002	-0.319	0.009	0.68	0.13	0.32	5273	169	142	8.95	1	
J150150-572144	T13	319.828	1.168	0.009	0.48	0.09	0.41	4756	135	102	8.71	1	
J150160-581343	T14	319.430	0.398	0.006	0.41	0.06	0.32	11828	138	113	9.43	1	
J150206-595406	T14	318.640	-1.076	0.004	0.37	0.05	0.34	12598	323	317	9.43	1	
J150209-592728	T14	318.858	-0.690	0.005	0.14	0.03	0.27	4162	37	23	8.06	2	
J150214-593405	T14	318.813	-0.791	0.011	1.21	0.17	0.33	5396	180	156	9.22	1	
J150234-574631	T13	319.715	0.759	0.008	0.74	0.11	0.37	5790	181	146	9.07	1	
J150245-592632	T14	318.933	-0.713	0.009	0.43	0.08	0.31	5459	45	45	8.79	1	
J150248-591258	T14	319.047	-0.518	0.006	0.21	0.03	0.30	11565	127	78	9.12	1	
J150304-572718	T14	319.928	1.007	0.004	0.14	0.03	0.31	4599	45	45	8.14	2	
J150320-573416	T13	319.904	0.888	0.006	0.77	0.08	0.34	18736	377	377	10.09	1	
J150345-571615	T14	320.098	1.124	0.005	0.20	0.03	0.36	14885	93	75	9.31	1	
J150406-590147	T14	319.282	-0.435	0.006	0.31	0.04	0.32	13005	89	62	9.39	1	
J150423-573757	T13	319.996	0.767	0.006	0.18	0.03	0.33	11992	46	46	9.07	1	
J150441-600535	T14	318.829	-1.400	0.054	4.66	0.66	0.60	4719	90	85	9.69	1	
J150444-571309	T13	320.238	1.105	0.034	4.48	0.64	0.47	3173	134	134	9.33	1	
J150451-590810	T14	319.314	-0.575	0.004	0.38	0.05	0.32	14237	279	246	9.55	1	
J150503-585842	T14	319.416	-0.451	0.005	0.30	0.04	0.29	16213	93	78	9.56	1	
J150554-583101	T13	319.738	-0.103	0.004	0.13	0.02	0.32	5229	81	68	8.21	1	
J150609-581012	T13	319.937	0.183	0.008	0.96	0.14	0.39	11997	225	187	9.81	1	
J150716-571931	T13	320.486	0.843	0.007	0.22	0.04	0.36	8672	125	82	8.89	1	
J150721-571817	T13	320.506	0.855	0.004	0.18	0.03	0.33	11486	92	84	9.05	1	
J150856-594552	T14	319.454	-1.379	0.015	0.66	0.12	0.72	4205	90	90	8.74	1	
J150857-573460	T13	320.553	0.506	0.027	3.95	0.56	0.43	5004	171	156	9.67	1	
J150901-572232	T13	320.665	0.681	0.012	0.78	0.11	0.39	11659	46	46	9.69	1	
J150913-580509	T13	320.330	0.054	0.017	1.77	0.25	0.47	5503	181	181	9.40	1	
J150919-564815	T13	320.986	1.155	0.019	0.75	0.14	0.40	4943	44	28	8.94	1	
J150921-581826	T13	320.235	-0.147	0.012	1.45	0.21	0.44	6390	192	134	9.45	1	
J150944-573852	T13	320.611	0.397	0.012	0.53	0.08	0.37	14061	46	46	9.68	2	
J151000-574844	T13	320.558	0.238	0.005	0.33	0.05	0.39	14108	158	80	9.48	2	
J151005-573635	T13	320.670	0.407	0.008	0.27	0.05	0.34	5849	82	51	8.63	1	
J151032-593156	T13	319.746	-1.280	0.007	0.21	0.03	0.52	20149	176	26	9.58	2	
J151035-581232	T13	320.424	-0.144	0.006	0.50	0.07	0.42	8234	216	179	9.20	2	
J151056-583150	T13	320.300	-0.444	0.003	0.24	0.03	0.37	12051	231	106	9.21	2	
J151058-574513	T13	320.699	0.222	0.011	1.03	0.15	0.47	13320	231	231	9.93	2	
J151112-565432	T13	321.156	0.934	0.007	0.31	0.04	0.33	8708	86	71	9.04	1	
J151120-572808	T13	320.886	0.443	0.008	0.33	0.06	0.37	4823	81	64	8.56	1	

## GA-SMGPS galaxy catalog –Continued.

SMGPS name J2000 (1)	Mosaic TXX (2)	$\ell$ deg (3)	$b$ deg (4)	$S_{\text{peak}}$ Jy (5)	$S_{\text{int}}$ Jy km/s (6)	$\text{err}_{S_{\text{int}}}$ Jy km/s (7)	RMS Jy km/s (8)	$V_{\text{hel}}$ km/s (9)	$W_{20}$ km/s (10)	$W_{50}$ km/s (11)	$\log M_{\text{HI}}$ $\log M_{\odot}$ (12)	Flag 1/2 (13)	Note or counterpart
J151122-575916	T13	320.625	-0.006	0.013	1.89	0.27	0.42	10415	319	228	9.98	1	
J151129-573716	T13	320.825	0.302	0.006	0.65	0.09	0.38	11921	323	323	9.63	1	
J151137-565952	T13	321.160	0.828	0.005	0.14	0.03	0.34	11506	184	166	8.94	1	
J151203-580238	T13	320.674	-0.100	0.005	0.54	0.08	0.39	12943	296	192	9.62	1	
J151212-584501	T13	320.328	-0.717	0.018	2.52	0.36	0.46	8150	137	137	9.89	1	
J151213-573919	T13	320.892	0.222	0.012	1.27	0.18	0.37	4935	177	139	9.16	1	
J151245-573906	T13	320.955	0.189	0.018	2.33	0.33	0.41	4911	211	180	9.43	1	
J151249-583555	T13	320.476	-0.628	0.022	4.44	0.63	0.45	4970	326	281	9.72	1	
J151252-575049	T13	320.868	0.013	0.005	0.19	0.04	0.33	5260	90	83	8.40	1	
J151311-571959	T13	321.170	0.431	0.009	1.09	0.15	0.35	4959	211	181	9.10	1	
J151326-574900	T13	320.948	0.001	0.013	0.85	0.16	0.36	3050	83	69	8.58	1	
J151331-581515	T13	320.733	-0.380	0.019	1.26	0.18	0.43	5420	45	45	9.24	1	
J151331-582633	T13	320.635	-0.542	0.015	0.84	0.12	0.42	11994	108	61	9.75	1	
J151349-570120	T13	321.404	0.654	0.021	1.19	0.17	0.35	4939	90	60	9.14	1	
J151350-582552	T13	320.676	-0.553	0.016	1.91	0.27	0.45	6232	207	115	9.54	1	
J151356-564906	T13	321.524	0.819	0.038	6.01	0.85	0.41	4956	256	219	9.84	1	
J151402-583936	T13	320.578	-0.762	0.007	0.86	0.12	0.42	11894	217	175	9.75	1	
J151406-564053	T13	321.614	0.924	0.012	1.09	0.15	0.40	6137	127	112	9.29	1	
J151420-575459	T13	321.000	-0.148	0.009	0.38	0.07	0.37	4782	45	45	8.62	1	
J151420-581116	T13	320.858	-0.379	0.005	1.03	0.15	0.42	12807	578	476	9.89	1	
J151421-560748	T13	321.930	1.378	0.009	0.42	0.08	0.58	5284	135	112	8.74	1	
J151422-572855	T13	321.229	0.221	0.008	0.64	0.09	0.38	10399	239	185	9.51	1	
J151426-565935	T13	321.490	0.635	0.006	0.26	0.05	0.26	4906	122	93	8.48	1	
J151427-585911	T13	320.457	-1.069	0.016	0.46	0.07	0.59	12070	81	50	9.49	1	
J151451-573517	T13	321.228	0.098	0.008	0.32	0.06	0.35	5315	62	33	8.64	1	
J151458-582906	T13	320.775	-0.676	0.010	0.69	0.10	0.41	13214	93	93	9.74	1	
J151513-585626	T13	320.565	-1.082	0.009	0.47	0.07	0.52	16316	176	103	9.76	2	
J151531-565924	T13	321.618	0.560	0.008	0.44	0.06	0.34	7172	135	103	9.02	1	
J151556-575060	T13	321.215	-0.201	0.017	0.82	0.12	0.40	5391	81	52	9.05	1	
J151711-581354	T13	321.155	-0.613	0.006	0.31	0.06	0.38	7700	182	182	8.93	1	
J151712-570428	T13	321.769	0.368	0.021	1.17	0.17	0.38	7044	82	68	9.44	1	
J151724-580948	T13	321.215	-0.570	0.006	0.22	0.04	0.39	6615	45	45	8.65	2	
J151738-573215	T13	321.572	-0.055	0.004	0.25	0.05	0.36	6717	162	116	8.72	1	
J151754-572156	T13	321.695	0.071	0.003	0.09	0.02	0.31	8014	83	69	8.43	2	
J151758-565527	T13	321.936	0.441	0.008	0.35	0.07	0.35	6408	91	74	8.83	1	
J151805-571152	T13	321.804	0.200	0.010	0.95	0.13	0.41	5225	131	116	9.09	1	
J151830-553858	T12	322.677	1.480	0.071	12.04	1.71	0.84	1510	257	237	9.12	1	
J151846-585113	T13	321.000	-1.250	0.016	1.61	0.16	0.53	13415	165	122	10.13	1	
J151853-584354	T13	321.078	-1.155	0.015	1.24	0.18	0.57	6034	156	116	9.33	2	
J151931-563454	T13	322.298	0.617	0.005	0.34	0.05	0.33	23422	181	161	9.92	1	
J151944-590145	T13	321.011	-1.465	0.018	1.31	0.18	0.83	5457	197	125	9.26	1	
J151946-563117	T13	322.360	0.649	0.011	1.16	0.16	0.36	5597	217	188	9.23	1	
J152008-572644	T13	321.905	-0.157	0.014	2.41	0.34	0.41	4937	219	204	9.44	1	
J152018-561112	T12	322.602	0.892	0.009	0.40	0.07	0.38	2820	81	67	8.18	1	
J152023-582036	T13	321.450	-0.932	0.009	0.48	0.09	0.43	5667	152	97	8.86	1	
J152029-574035	T13	321.821	-0.377	0.007	0.20	0.04	0.31	5448	43	27	8.45	1	
J152036-554913	T12	322.836	1.177	0.009	0.46	0.07	0.42	9477	75	47	9.29	1	
J152057-570827	T13	322.163	0.040	0.007	0.44	0.08	0.35	5549	135	135	8.80	1	
J152107-580100	T13	321.708	-0.709	0.007	0.23	0.04	0.36	5367	45	45	8.49	1	
J152120-571618	T13	322.136	-0.098	0.005	0.11	0.02	0.32	5223	45	35	8.17	2	
J152134-572049	T13	322.121	-0.178	0.009	0.99	0.14	0.38	5087	135	135	9.08	1	
J152138-561613	T12	322.713	0.721	0.011	1.62	0.23	0.39	7385	256	221	9.62	1	
J152228-573544	T13	322.087	-0.453	0.006	0.45	0.06	0.36	10859	184	184	9.39	1	
J152240-575642	T13	321.919	-0.760	0.012	1.69	0.24	0.42	5374	441	101	9.36	2	
J152245-573047	T13	322.165	-0.405	0.005	0.17	0.03	0.31	5645	89	65	8.41	1	

## GA-SMGPS galaxy catalog –Continued.

SMGPS name J2000 (1)	Mosaic TXX (2)	$\ell$ deg (3)	$b$ deg (4)	$S_{\text{peak}}$ Jy (5)	$S_{\text{int}}$ Jy km/s (6)	$\text{err}_{S_{\text{int}}}$ Jy km/s (7)	RMS Jy km/s (8)	$V_{\text{hel}}$ km/s (9)	$W_{20}$ km/s (10)	$W_{50}$ km/s (11)	$\log M_{\text{HI}}$ $\log M_{\odot}$ (12)	Flag 1/2 (13)	Note or counterpart
J152306-575237	T13	322.006	-0.735	0.008	0.55	0.10	0.36	6014	169	151	8.97	1	
J152356-571756	T13	322.416	-0.313	0.007	0.49	0.09	0.33	5142	125	92	8.79	1	
J152404-583314	T13	321.740	-1.370	0.027	2.11	0.30	0.70	3389	127	113	9.06	1	
J152425-565509	T12	322.680	-0.032	0.023	4.50	0.64	0.42	5306	304	279	9.78	1	
J152448-570610	T12	322.622	-0.213	0.010	0.93	0.13	0.37	6765	136	119	9.30	1	
J152450-560322	T12	323.203	0.656	0.010	0.41	0.06	0.34	7972	79	61	9.08	1	
J152502-552507	T12	323.579	1.172	0.005	0.12	0.02	0.37	16541	86	59	9.18	2	
J152528-580743	T13	322.128	-1.117	0.008	0.87	0.16	0.44	4307	238	173	8.89	1	
J152529-561620	T12	323.159	0.427	0.005	0.25	0.05	0.30	6986	181	162	8.77	1	
J152534-580047	T13	322.204	-1.029	0.013	1.14	0.16	0.43	5692	173	159	9.24	1	
J152559-570439	T12	322.770	-0.282	0.013	1.26	0.18	0.34	5330	164	143	9.23	1	
J152615-571822	T12	322.673	-0.492	0.035	1.55	0.22	0.37	6461	77	48	9.48	1	
J152622-564741	T12	322.970	-0.075	0.026	3.47	0.49	0.37	5365	205	149	9.67	1	
J152627-554910	T12	323.523	0.728	0.007	0.40	0.06	0.32	7960	136	120	9.07	1	
J152629-555608	T12	323.462	0.629	0.017	1.27	0.18	0.32	5299	174	92	9.23	1	
J152634-563346	T12	323.122	0.102	0.009	0.77	0.11	0.32	14437	358	299	9.87	1	
J152635-574240	T12	322.485	-0.854	0.008	0.27	0.05	0.37	4913	45	45	8.48	1	
J152635-581313	T13	322.199	-1.275	0.007	0.14	0.03	0.50	5046	45	45	8.24	2	
J152649-565704	T12	322.934	-0.240	0.008	1.01	0.14	0.33	6069	222	198	9.24	1	
J152700-563247	T12	323.182	0.081	0.005	0.54	0.08	0.31	14553	262	232	9.72	1	
J152722-550244	T12	324.064	1.297	0.022	2.43	0.45	0.55	2785	168	133	8.95	1	
J152734-571756	T12	322.825	-0.585	0.008	0.67	0.12	0.36	5409	171	157	8.97	1	
J152743-574825	T12	322.556	-1.018	0.007	0.20	0.04	0.36	5087	45	37	8.38	1	
J152819-572530	T12	322.836	-0.746	0.022	1.13	0.16	0.36	5383	103	58	9.19	1	
J152835-570209	T12	323.086	-0.445	0.005	0.19	0.04	0.29	5179	112	68	8.39	1	
J152900-570743	T12	323.081	-0.554	0.017	1.70	0.24	0.36	6598	178	146	9.54	1	
J152908-573340	T12	322.850	-0.920	0.017	2.05	0.29	0.36	5107	225	180	9.40	1	
J152919-565236	T12	323.259	-0.371	0.006	0.34	0.05	0.30	10374	131	94	9.23	1	
J152945-570653	T12	323.172	-0.600	0.008	0.48	0.09	0.31	4599	120	88	8.68	1	
J152950-571146	T12	323.135	-0.673	0.004	0.31	0.06	0.29	5225	214	177	8.60	1	
J153001-580438	T12	322.654	-1.412	0.025	1.27	0.18	0.73	5538	90	68	9.26	1	
J153034-554622	T12	324.027	0.441	0.006	0.64	0.09	0.33	7086	268	251	9.18	1	
J153037-554054	T12	324.085	0.512	0.056	14.66	1.44	0.41	5000	335	240	10.24	1	
J153045-580625	T12	322.718	-1.492	0.050	3.03	0.43	0.90	4983	90	90	9.55	1	
J153059-554628	T12	324.074	0.406	0.009	0.83	0.12	0.35	14625	314	296	9.91	1	
J153113-545247	T12	324.614	1.120	0.007	0.31	0.04	0.40	8324	91	91	9.00	1	
J153115-560152	T12	323.958	0.174	0.033	1.43	0.27	0.31	1856	39	24	8.37	1	
J153123-545517	T12	324.609	1.073	0.010	1.08	0.11	0.43	19051	235	197	10.25	1	
J153123-572009	T12	323.228	-0.908	0.011	0.67	0.10	0.35	14200	103	77	9.79	1	
J153125-555213	T12	324.069	0.293	0.022	2.40	0.34	0.38	4900	131	116	9.43	1	
J153146-574202	T12	323.061	-1.235	0.007	0.38	0.05	0.41	10426	183	168	9.28	1	
J153149-553838	T12	324.246	0.445	0.050	4.08	0.76	0.34	1466	119	85	8.62	1	
J153151-570406	T12	323.432	-0.724	0.017	0.74	0.14	0.34	4902	45	33	8.92	1	
J153213-574659	T12	323.063	-1.338	0.017	0.62	0.12	0.48	5486	85	53	8.95	1	
J153214-560042	T12	324.082	0.111	0.006	0.84	0.16	0.32	4956	328	275	8.99	1	
J153231-563513	T12	323.783	-0.382	0.010	0.60	0.11	0.34	5372	119	91	8.92	1	
J153258-555431	T12	324.226	0.136	0.004	0.24	0.03	0.30	9828	183	167	9.04	1	
J153320-554726	T12	324.337	0.202	0.007	0.50	0.09	0.32	5033	127	109	8.78	1	
J153334-544713	T12	324.942	1.003	0.020	1.16	0.22	0.37	2691	45	45	8.60	1	
J153429-560942	T12	324.252	-0.193	0.035	4.45	0.63	0.41	2884	170	136	9.25	1	
J153512-564945	T12	323.944	-0.794	0.013	0.40	0.13	0.30	1400	75	47	7.57	2	
J153516-542147	T12	325.389	1.205	0.029	5.39	0.77	0.55	5696	260	240	9.92	1	
J153520-550207	T12	325.006	0.652	0.016	0.66	0.12	0.36	2759	105	60	8.38	1	
J153525-571159	T12	323.751	-1.111	0.007	0.41	0.08	0.38	4660	128	108	8.62	1	
J153529-553408	T12	324.711	0.207	0.006	0.35	0.07	0.31	5404	90	90	8.69	1	

## GA-SMGPS galaxy catalog –Continued.

SMGPS name J2000 (1)	Mosaic TXX (2)	$\ell$ deg (3)	$b$ deg (4)	$S_{\text{peak}}$ Jy (5)	$S_{\text{int}}$ Jy km/s (6)	$\text{err}_{S_{\text{int}}}$ Jy km/s (7)	RMS Jy km/s (8)	$V_{\text{hel}}$ km/s (9)	$W_{20}$ km/s (10)	$W_{50}$ km/s (11)	$\log M_{\text{HI}}$ $\log M_{\odot}$ (12)	Flag 1/2 (13)	Note or counterpart
J153537-551035	T12	324.956	0.515	0.006	0.30	0.06	0.33	7338	91	91	8.88	1	
J153542-551656	T12	324.903	0.422	0.017	0.74	0.11	0.34	15985	47	47	9.94	1	
J153601-565327	T12	323.998	-0.908	0.005	0.30	0.04	0.31	14235	130	116	9.45	1	
J153625-543228	T12	325.422	0.962	0.016	2.10	0.21	0.39	10433	225	196	10.03	1	
J153630-562544	T12	324.322	-0.572	0.087	18.01	2.56	0.43	2706	179	179	9.80	1	J1536-56
J153636-543914	T12	325.376	0.856	0.017	2.27	0.22	0.39	10394	183	165	10.06	1	two sources?
J153658-563846	T12	324.247	-0.786	0.018	3.18	0.45	0.40	5077	346	316	9.59	1	
J153712-542517	T12	325.583	0.992	0.006	0.17	0.02	0.32	21888	95	45	9.57	1	
J153728-554334	T12	324.846	-0.085	0.003	0.09	0.02	0.30	5795	72	42	8.13	2	
J153736-542754	T12	325.605	0.923	0.009	0.63	0.12	0.34	5674	90	90	8.98	1	
J153757-570048	T12	324.139	-1.163	0.008	0.26	0.05	0.38	3331	45	31	8.14	2	
J153803-544859	T12	325.450	0.600	0.005	0.17	0.03	0.26	10496	92	92	8.94	2	
J153809-571412	T12	324.029	-1.359	0.007	0.39	0.06	0.47	16201	125	101	9.67	1	
J153815-540623	T11	325.894	1.155	0.010	0.77	0.11	0.33	9192	137	137	9.48	1	
J153846-555147	T12	324.912	-0.303	0.014	1.29	0.18	0.38	5806	128	114	9.31	1	
J153848-544617	T12	325.564	0.572	0.030	3.78	0.54	0.37	2620	187	145	9.09	1	
J153853-542139	T12	325.817	0.896	0.003	0.09	0.01	0.28	21529	95	70	9.27	1	
J153921-554142	T12	325.077	-0.216	0.012	1.40	0.20	0.38	11126	265	248	9.90	1	
J153958-563531	T12	324.612	-0.988	0.026	4.25	0.60	0.46	5475	226	213	9.78	1	
J154034-540015	T11	326.228	1.035	0.012	1.17	0.17	0.38	9243	221	207	9.67	1	
J154052-564049	T12	324.658	-1.132	0.012	1.11	0.16	0.47	6201	136	136	9.30	1	
J154105-551503	T12	325.540	-0.007	0.006	0.14	0.03	0.31	6465	73	45	8.45	2	
J154108-554414	T12	325.254	-0.401	0.009	0.79	0.11	0.40	5803	163	123	9.10	2	
J154210-540421	T11	326.375	0.839	0.005	0.28	0.04	0.37	16152	172	134	9.53	2	
J154302-533060	T11	326.812	1.205	0.015	0.95	0.13	0.51	10320	247	169	9.67	2	two galaxies?
J154306-551947	T11	325.721	-0.243	0.031	2.14	0.30	0.40	5411	142	77	9.47	1	J1542-55
J154318-560902	T12	325.246	-0.913	0.006	0.53	0.10	0.37	5867	136	121	8.93	1	
J154337-555404	T12	325.432	-0.741	0.007	1.26	0.18	0.39	5698	309	278	9.29	1	
J154404-532444	T11	326.999	1.194	0.017	1.29	0.18	0.45	10415	138	129	9.81	1	
J154417-555233	T12	325.522	-0.778	0.003	0.09	0.02	0.33	10365	46	46	8.65	2	
J154419-553709	T12	325.682	-0.578	0.016	1.04	0.15	0.39	5582	114	71	9.19	1	
J154421-532457	T11	327.029	1.166	0.013	0.81	0.12	0.41	9006	137	109	9.49	1	
J154437-543819	T11	326.314	0.173	0.014	1.85	0.26	0.40	5972	267	247	9.49	1	
J154512-545328	T11	326.226	-0.078	0.027	6.70	0.66	0.45	6565	563	310	10.13	1	
J154515-561616	T12	325.388	-1.174	0.023	2.91	0.41	0.57	5479	207	162	9.61	1	J1545-56
J154519-550344	T11	326.135	-0.224	0.016	2.52	0.36	0.42	6472	217	189	9.70	1	
J154524-532812	T11	327.120	1.028	0.006	0.77	0.11	0.34	8851	319	319	9.45	2	
J154658-542652	T11	326.700	0.115	0.015	2.08	0.08	0.49	16701	209	99	10.42	2	
J154805-554957	T12	325.969	-1.072	0.007	0.48	0.21	0.40	12631	180	118	9.55	1	
J154811-560411	T11	325.834	-1.267	0.018	0.98	0.07	0.50	5264	90	77	9.11	1	
J154827-554146	T11	326.094	-0.997	0.020	2.77	0.07	0.49	10446	367	330	10.15	1	
J154843-554708	T11	326.068	-1.091	0.009	0.47	0.14	0.47	5617	90	89	8.85	1	
J154851-534552	T11	327.340	0.480	0.007	0.49	0.27	0.38	17731	235	195	9.85	1	
J154914-532948	T11	327.551	0.655	0.011	0.76	0.09	0.38	8688	127	96	9.43	1	
J154916-544125	T11	326.811	-0.282	0.007	0.37	0.11	0.40	10655	138	138	9.29	1	
J154921-535126	T11	327.340	0.362	0.006	0.53	0.05	0.38	17793	320	306	9.89	1	
J154949-532314	T11	327.688	0.686	0.015	0.55	0.08	0.35	10834	46	33	9.48	1	
J154950-560940	T12	325.956	-1.481	0.051	7.38	1.05	0.95	5256	433	403	9.98	1	
J155009-532052	T11	327.751	0.685	0.005	0.14	0.03	0.31	8860	46	46	8.72	2	
J155059-541853	T11	327.242	-0.146	0.008	0.21	0.04	0.54	9080	137	30	8.90	2	
J155145-542051	T11	327.307	-0.241	0.004	0.30	0.04	0.43	16079	140	140	9.54	2	
J155205-533807	T11	327.795	0.281	0.010	0.43	0.06	0.44	10060	92	64	9.31	1	
J155221-542413	T11	327.340	-0.340	0.009	0.35	0.19	0.38	16975	86	71	9.66	1	
J155249-535258	T11	327.723	0.020	0.021	1.33	0.54	0.44	5972	82	64	9.35	1	wide DH?
J155327-550850	T11	326.992	-1.016	0.032	3.83	0.05	0.60	5678	329	221	9.77	2	

## GA-SMGPS galaxy catalog –Continued.

SMGPS name J2000 (1)	Mosaic TXX (2)	$\ell$ deg (3)	$b$ deg (4)	$S_{\text{peak}}$ Jy (5)	$S_{\text{int}}$ Jy km/s (6)	$\text{err}_{S_{\text{int}}}$ Jy km/s (7)	RMS Jy km/s (8)	$V_{\text{hel}}$ km/s (9)	$W_{20}$ km/s (10)	$W_{50}$ km/s (11)	$\log M_{\text{HI}}$ $\log M_{\odot}$ (12)	Flag 1/2 (13)	Note or counterpart
J155334-545518	T11	327.148	-0.852	0.006	5.00	0.49	0.63	12436	502	468	10.55	1	
J155416-544431	T11	327.340	-0.778	0.005	0.36	0.10	0.49	12576	171	85	9.42	2	
J155431-525047	T11	328.576	0.660	0.005	0.69	0.80	0.33	6186	348	258	9.10	1	
J155440-532329	T11	328.246	0.226	0.034	8.10	0.19	0.43	6082	475	444	10.15	1	
J155442-553036	T11	326.898	-1.409	0.016	1.01	0.10	0.71	2654	121	90	8.53	2	
J155444-530555	T11	328.440	0.444	0.015	0.73	0.09	0.37	10458	46	46	9.57	1	
J155449-515951	T11	329.153	1.285	0.008	0.65	0.04	0.53	6311	226	206	9.09	1	
J155508-530514	T11	328.494	0.415	0.008	0.31	0.28	0.35	10564	78	40	9.21	1	
J155525-520823	T10	329.134	1.115	0.011	1.99	0.13	0.44	6390	264	250	9.58	1	
J155615-534711	T11	328.173	-0.228	0.012	0.89	0.17	0.47	7920	165	135	9.42	1	
J155646-522241	T10	329.139	0.800	0.007	1.23	0.72	0.39	6437	317	296	9.38	1	
J155723-522117	T10	329.225	0.758	0.024	7.35	0.40	0.43	6190	488	457	10.12	1	
J155726-514535	T10	329.616	1.206	0.015	2.84	0.03	0.52	6653	476	410	9.77	1	
J155742-530912	T11	328.746	0.117	0.007	0.18	0.06	0.38	10299	37	23	8.95	2	
J155744-535616	T11	328.243	-0.485	0.008	0.44	0.31	0.42	7711	261	218	9.08	2	
J155816-523922	T10	329.134	0.440	0.018	2.15	0.05	0.39	6080	191	145	9.57	1	
J155824-514727	T10	329.710	1.086	0.009	0.29	0.94	0.36	6179	36	23	8.71	2	
J155827-535530	T11	328.331	-0.543	0.031	6.64	0.47	0.50	5359	429	385	9.95	1	
J155843-540025	T11	328.308	-0.631	0.025	3.30	0.05	0.47	5418	251	236	9.66	1	
J155857-520212	T10	329.615	0.844	0.010	1.53	0.22	0.40	6313	217	201	9.46	1	
J155905-534316	T11	328.536	-0.449	0.015	1.88	0.27	0.52	10243	355	322	9.96	1	
J155918-543608	T11	327.986	-1.139	0.025	3.40	0.48	0.58	5582	232	176	9.70	1	
J155953-530508	T10	329.039	-0.044	0.019	4.19	0.59	0.44	5542	333	276	9.78	1	
J160000-540902	T11	328.359	-0.863	0.016	0.83	0.12	0.43	5727	82	58	9.11	1	
J160117-531138	T10	329.127	-0.263	0.007	0.56	0.10	0.40	5479	127	113	8.90	1	
J160124-532600	T10	328.984	-0.456	0.013	1.75	0.25	0.41	5472	203	162	9.39	1	
J160133-532940	T10	328.961	-0.517	0.010	1.13	0.16	0.45	10417	271	204	9.75	2	
J160143-530724	T10	329.223	-0.253	0.005	0.60	0.09	0.39	5986	248	193	9.01	1	
J160211-522441	T10	329.744	0.237	0.007	0.56	0.08	0.40	6657	177	161	9.07	1	
J160220-512602	T10	330.406	0.957	0.020	2.89	0.41	0.45	5968	207	160	9.69	1	
J160234-511356	T10	330.566	1.085	0.008	1.35	0.19	0.42	10214	321	269	9.82	1	
J160307-531754	T10	329.265	-0.523	0.033	3.56	0.51	0.38	5790	157	103	9.75	1	
J160316-511701	T10	330.614	0.974	0.011	0.56	0.08	0.36	6428	45	45	9.03	1	
J160346-512045	T10	330.632	0.875	0.013	1.79	0.18	0.38	16685	187	159	10.36	1	
J160419-513418	T10	330.545	0.651	0.011	1.37	0.19	0.35	5959	181	181	9.36	1	
J160429-514229	T10	330.474	0.531	0.012	1.04	0.15	0.38	8688	182	147	9.57	1	
J160502-523119	T10	329.996	-0.132	0.007	1.07	0.11	0.37	14462	221	187	10.01	1	
J160508-523621	T10	329.952	-0.205	0.013	1.56	0.22	0.40	6038	181	152	9.43	1	
J160511-514636	T10	330.510	0.408	0.017	3.03	0.30	0.42	16883	262	218	10.59	1	
J160523-522354	T10	330.119	-0.076	0.008	1.34	0.19	0.40	6177	359	326	9.38	1	
J160547-511331	T10	330.946	0.757	0.017	4.48	0.64	0.44	5716	383	334	9.84	1	
J160623-532430	T10	329.556	-0.928	0.010	0.70	0.10	0.36	5891	110	80	9.06	1	
J160625-502618	T10	331.547	1.275	0.010	1.70	0.17	0.59	16152	187	187	10.31	1	
J160648-525135	T10	329.971	-0.564	0.009	0.47	0.09	0.35	5692	77	57	8.86	1	
J160710-514941	T10	330.704	0.164	0.013	1.35	0.19	0.45	5929	201	137	9.35	1	
J160722-534156	T10	329.469	-1.242	0.012	1.10	0.16	0.53	5665	130	108	9.22	1	
J160727-503356	T10	331.583	1.071	0.008	0.75	0.11	0.44	6371	147	90	9.16	2	
J160732-534914	T10	329.406	-1.349	0.039	6.95	0.99	0.76	5483	342	265	9.99	1	
J160736-523311	T10	330.266	-0.417	0.009	0.47	0.07	0.38	14404	46	46	9.65	1	
J160744-530122	T10	329.965	-0.779	0.011	2.09	0.30	0.37	5667	313	292	9.50	1	
J160747-522509	T10	330.377	-0.338	0.005	0.54	0.10	0.36	5637	135	135	8.91	1	
J160748-510447	T10	331.280	0.652	0.054	8.72	0.86	0.52	6036	212	181	10.18	1	
J160756-504534	T10	331.511	0.875	0.013	1.43	0.20	0.47	5825	172	158	9.36	1	
J160802-505204	T10	331.449	0.785	0.009	0.97	0.14	0.45	6287	135	115	9.26	1	
J160855-530935	T10	330.003	-0.999	0.017	3.70	0.36	0.40	10464	321	313	10.27	1	

## GA-SMGPS galaxy catalog –Continued.

SMGPS name J2000 (1)	Mosaic TXX (2)	$\ell$ deg (3)	$b$ deg (4)	$S_{\text{peak}}$ Jy (5)	$S_{\text{int}}$ Jy km/s (6)	$\text{err}_{S_{\text{int}}}$ Jy km/s (7)	RMS Jy km/s (8)	$V_{\text{hel}}$ km/s (9)	$W_{20}$ km/s (10)	$W_{50}$ km/s (11)	$\log M_{\text{HI}}$ $\log M_{\odot}$ (12)	Flag 1/2 (13)	Note or counterpart
J160912-501849	T10	331.960	1.068	0.034	3.80	0.54	0.48	6450	158	121	9.87	1	
J160927-504618	T10	331.680	0.704	0.011	3.50	0.50	0.49	5740	497	491	9.74	1	
J160937-501628	T10	332.035	1.053	0.014	2.27	0.22	0.51	14565	307	150	10.34	1	
J160942-503332	T10	331.853	0.833	0.015	2.28	0.32	0.41	6384	177	162	9.64	1	
J160957-515226	T10	330.991	-0.160	0.006	0.21	0.04	0.39	5865	45	31	8.54	2	
J161003-525106	T10	330.339	-0.889	0.010	1.64	0.16	0.40	14207	371	335	10.18	1	
J161008-501125	T10	332.152	1.059	0.032	5.68	0.56	0.58	6245	222	184	10.02	1	
J161037-511135	T10	331.528	0.270	0.006	0.48	0.09	0.48	5394	149	101	8.82	1	
J161124-502402	T10	332.158	0.767	0.008	0.50	0.07	0.42	9349	137	115	9.31	1	
J161246-524516	T10	330.705	-1.097	0.025	2.81	0.40	0.45	5678	155	114	9.63	1	
J161431-521457	T10	331.246	-0.913	0.009	0.93	0.13	0.42	10614	242	63	9.69	2	
J161530-521221	T10	331.384	-0.985	0.010	1.01	0.14	0.44	5641	194	143	9.18	1	
J161622-520039	T10	331.615	-0.937	0.009	0.42	0.08	0.39	5153	84	69	8.72	1	
J161711-521634	T10	331.520	-1.214	0.019	2.76	0.39	0.60	5153	203	167	9.54	1	
J161742-520101	T10	331.758	-1.084	0.014	1.05	0.15	0.44	5232	119	89	9.13	1	
J161833-520837	T10	331.764	-1.267	0.017	2.51	0.25	0.58	10995	230	230	10.15	1	

<sup>1</sup>Consists of a galaxy A ( $V_{\text{hel}} \approx 16483 - 16532$  km/s), which could be a close pair, plus an offset neighbour B ( $V_{\text{hel}} \approx 16928$  km/s).<sup>2</sup>Special case: very extended on-sky. The dispersed emission does not appear clear in the moment maps.<sup>3</sup>Other names: IRAS 15147-5527 and WISEA J151829.66-553849.4

This paper has been typeset from a  $\text{\TeX}/\text{\LaTeX}$  file prepared by the author.